EXTRAPOLATION OF TEST PERFORMANCE FOR AIR-TO-AIR ROTARY ENERGY EXCHANGERS

by

Alaa Jamal Alhariry

A thesis submitted to the faculty of
The University of North Carolina at Charlotte
in partial fulfillment of the requirements
for the degree of Master of Science in
Applied Energy and Electromechanical Systems

Charlotte

2022

Approved by:

_____
Dr. Weimin Wang

_____
Dr. Wesley Williams

_____
Dr. Elizabeth Smith

ABSTRACT

Alaa Jamal Alhariry. Extrapolation of Test Performance for Air-to-Air Rotary Energy Exchangers. (Under the direction of Dr. WEIMIN WANG)

Air-to-air energy exchangers are used in building HVAC systems to transfer energy between the exhaust air and the outdoor air. Because of its potential to reduce the energy consumption for conditioning ventilation air and to downsize the cooling and heating equipment, air-to-air energy recovery is required for use in many situations according to the prevalent energy efficiency standards (e.g., ASHRAE Standard 90.1) for commercial buildings. Typically, the performance of air-to-air energy exchangers is tested, rated and certified according to industry-accepted standards and procedures such as ASHRAE Standard 84 and AHRI Standard 1060. Because of the expenses and facility constraints associated with laboratory testing, performance rating tests of air-to-air energy exchangers are usually performed at a limited set of standard test conditions for selected products. However, manufacturers may produce a large variety of products with different sizes and energy exchangers may operate in the field under operating conditions different from those in the rating tests. There is a need to extrapolate the test results from small energy exchangers to large ones and from one operating condition to another. This research uses laboratory tests to validate the current extrapolation approach used by AHRI Standard 1060 and the performance correlation equation proposed in literature.

Two sets of air-to-air energy wheels from different manufacturers were selected for laboratory testing. Each set included three wheels of different sizes (i.e., small, medium, and large). The tests were performed at the AHRI-certified energy recovery testing facility at Intertek. Each set of wheels had a total 19 laboratory tests covering different test conditions for

effectiveness, leakage performance and pressure drop. The analysis of test results showed an overlap in performance ratings between different wheel sizes after accounting for allowable allowances, which in return supported the use of AHRI's extrapolation approach for performance rating. In addition, the test results were used to validate the selected effectiveness correlations from the literature. It was found that the latent effectiveness correlation matched well with the test results, but a modification of the sensible effectiveness correlation was necessary to match well with the test results. A customized model was developed in EnergyPlus to investigate the impact of operating conditions on annual energy simulation. The simulation of a standalone retail building in Atlanta, GA showed that ignoring the impact of operating conditions on exchanger effectiveness had a negligible impact on cooling energy consumption, but had 5%-18% more heating energy consumption than the model that considered the impact of operating conditions on exchanger effectiveness.

ACKNOWLEDGEMENTS

First of all, I would like to thank God for giving me the opportunity and guidance to achieve my goal and succeed in this part. My sincerest gratitude goes to Dr. Weimin Wang for the constant support, patience, motivation, enthusiasm, and immense knowledge from the beginning to the completion of this thesis. He kept me motivated by showing me how important it is for the quality of work to triumph over quantity, but his continuous care for my well-being kept me going. I am as thankful to Dr. Wesley Williams and Dr. Elizabeth Smith for their helpful suggestions to accomplish the thesis.

I would like to acknowledge the financial support offered by the American Society of Heating, Refrigerating and Air-Conditioning Engineering (ASHRAE) through the research project RP-1799. The laboratory tests were performed by Intertek. The Project Monitoring Subcommittee (PMS) of ASHRAE RP-1799 provided critical inputs and guidance.

Last but not least, I am forever grateful to my parents, relatives, and wife for giving me the support and strength to finish this thesis.

DEDICATION

This thesis is dedicated to my beloved parents and lovely wife.

Table of Contents

LIST OF TABLES

LIST OF FIGURES

Chapter 1: Introduction

1.1 Problem Statement

Global warming and many other environmental challenges have made it urgent for all countries in the world to reduce the consumption of fossil fuels and related carbon emissions. The Glasgow Climate Pact, published at the end of the 2021 United Nations Climate Change Conference (COP26), calls on all countries to strengthen their emissions-cutting plans to limit global warming to 1.5℃ above preindustrial levels. So far, countries covering more than 87% of global carbon emissions have set net-zero targets, although with differing time frames (Nugent 2021). In this respect, the U.S. aims to achieve about 50% reduction of greenhouse gas emissions from the 2005 levels in 2030 and reach net zero emissions by 2050.

Buildings are major energy consumers and carbon emitters. According to IEA (2019), the building sector accounts for about 30% of final energy use, more than 55% of global electricity consumption, and 28% of global energy-related CO_2 emissions. In the U.S., buildings consumed about 40% of the total energy consumption in 2020, with about 22% from the residential sector and 18% from the commercial sector (EIA 2021). Of the building energy end uses, heating, ventilation, and air conditioning (HVAC) accounts for 40-60% of the energy consumption in buildings (Zeng 2017). Therefore, using energy-efficient HVAC equipment and systems is important towards the reduction of energy consumption and carbon emissions in buildings.

Air-to-air energy recovery is an energy efficient technology for building HVAC systems. During building operation, fresh outdoor air needs to be supplied to the building to meet the minimum ventilation requirements as prescribed in ASHRAE Standards 62 (ASHRAE 2019a). The outdoor air is usually conditioned (heated/humidified in winter and cooled/dehumidified in summer) before it is sent to the occupied spaces. Conditioning outdoor air becomes part of the

load of heating and cooling equipment (i.e., furnace, compressor, heating and cooling coils) and consumes a lot of energy, especially when a large amount of outdoor air is required. Meanwhile, conditioned space air is exhausted to the ambient at a flow rate close to that for the outdoor air intake. Because the exhausted air is conditioned, it can be used to preheat or precool the outdoor air, which is the underlying concept of air-to-air energy recovery. By transferring energy between the exhaust air and the outdoor air, air-to-air energy recovery has the potential to significantly reduce the energy consumed to condition ventilation air. It also enables the downsizing of cooling and heating equipment, resulting in capital cost reduction. Using energy recovery is required in many situations according to the industry energy efficiency standards for commercial buildings, such as ASHRAE 90.1 (ASHRAE 2019b) and IGCC (ICC 2018).

Air-to-air energy exchangers come in different types and sizes, and they are categorized based on geometry, construction type, heat transfer, and the number of fluids. Common types include rotary wheels, heat pipes, recuperators, and run-around loops.

The performance of air-to-air energy recovery is an important consideration to determine the cost-effectiveness of deploying energy recovery in HVAC system design. Typically, the performance of air-to-air energy exchangers is tested, rated and certified according to industry-accepted standards and procedures. These standards and procedures may vary with countries and regions. In North America, ASHRAE Standard 84 (ASHRAE 2020a) sets the uniform laboratory testing method to obtain the effectiveness of air-to-air energy exchangers. Based on ASHRAE Standard 84, AHRI Standard 1060 (AHRI 2018) defines conditions and procedures for rating and certifying the performance of air-to-air exchangers for energy recovery.

Because of the expenses and facility constraints associated with laboratory testing, performance rating tests of air-to-air energy exchangers are usually performed at a limited set of

standard test conditions for selected products. However, manufacturers may produce a large variety of products with different sizes and energy exchangers may operate in the field under operating conditions (i.e., inlet air temperature, humidity, and flow rate) different from those in the rating tests. For example, large rotary wheels are available on the market to accommodate air flow rates up to the range from 23.6 m^3/s to 33 m^3/s. However, the two independent laboratory testing facilities (i.e., Intertek Testing Laboratory in Cortland, NY and Lucerne Laboratory in Switzerland) can only accommodate air flow rates up to 2.1 m^3/s. Therefore, it is not feasible to obtain the performance of large air-to-air energy exchange based on laboratory tests. There is a need to extrapolate the test results from small energy exchangers to large ones.

The Operations Manual of AHRI Standard 1060 (AHRI 2018) allows large air-to-air energy exchangers with nominal air flow rates above 2.36 m^3/s to be rated the same as a smaller exchanger (less than 2.36 m^3/s) if both large and small exchangers are in the same Basic Model Group (i.e., same design and construction). However, the validity of extrapolating rating tests of small exchangers to larger exchangers in the above manner has not been established in the open technical literature.

Simulation programs are widely used by building designers to evaluate energy efficiency technologies, including air-to-air energy recovery. To model air-to-air energy exchangers, performance curves or the performance values at standard test conditions are usually required by the simulation programs. Most practitioners assume the certified performance of energy exchangers apply to a broad range of conditions that are encountered in field operation, as implied in many energy simulation software such as EnergyPlus. However, laboratory studies are missing to evaluate the extent to which the heat exchanger performance varies with inlet air conditions.

1.2 Objectives

This research has the following objectives:

- Review the methods used in literature to correlate the performance of air-to-air energy exchangers with different sizes and operating conditions.
- Evaluate the impact of energy exchanger sizes on performance based on laboratory testing results.
- Evaluate the impact of energy exchanger operating conditions (i.e., inlet air temperature and humidity) on performance based on laboratory testing results.
- Compare the laboratory testing results with the correlations published in literature.
- Use the EnergyPlus software to estimate how much difference of simulated energy consumption can be caused by ignoring the impact of operating conditions on the performance of air-to-air energy exchangers.

1.3 Scope of Work

This thesis is based on the research project RP-1799 funded by ASHRAE. As the leading organization of ASHRAE Research Project RP-1799, Intertek is responsible for the laboratory tests of energy exchangers, while UNCC is responsible for providing technical support on commercial exchanger selection for testing, and test data analysis. In ASHRAE RP-1799, two sets of enthalpy wheels and two single enthalpy plate exchangers have been tested. This thesis covers only the two sets of enthalpy wheels. Specifically, the scope of my thesis work includes:

- Review the methods used in literature to correlate the performance of enthalpy wheels with different sizes and operating conditions.
- Compile and analyze the laboratory test data from Intertek.

- Evaluate the AHRI extrapolation approach of performance rating for large wheels based on the test results analysis.
- Evaluate the impact of energy exchanger operating conditions (i.e., inlet air temperature and humidity) on performance based on the test results analysis.
- Use the laboratory testing results to validate the wheel performance correlations published in literature.
- Develop building simulation models and use the EnergyPlus software (a whole-building simulation program developed by the U.S. Department of Energy) to estimate the difference of annual energy consumption between two scenarios: one scenario considering the impact of operating conditions on the wheel effectiveness and the other scenario not.

1.4 Thesis Organization

The thesis is organized in six chapters. Following this chapter of introduction, the remaining five chapters include the following: Chapter 2 provides a literature review. An overview of energy exchanger performance metrics, standards for exchanger testing and rating, and existing methods for extrapolation and correlation of exchanger performance are discussed. Chapter 3 describes the exchangers selected for testing and the testing conditions. The rationales behind the selection and the experimental design are discussed. Chapter 4 presents the laboratory test results and analysis. Processed test results (i.e., effectiveness and uncertainty) are summarized and analyzed to evaluate how the performance changes from small exchangers to large ones, and from one test condition to another. The test results are also used to verify one correlation model reviewed in Chapter 2. Chapter 5 covers the building model and the

EnergyPlus simulation results. Chapter 6 concludes the study and provide suggestions for future work.

Chapter 2: Literature Review

The literature review includes three subsections. First, an overview of air-to-air energy exchangers is provided by covering different types of air-to-air energy exchangers, the operating conditions, and the performance matrices. Then, the industry standards for testing and rating air-to-air heat exchangers are discussed. The third section describes extrapolation approaches and why it is needed, Technical Similarity Groups (TSGs), and related numerical models.

2.1 Overview of Air-to-Air Energy Exchangers

An air-to-air energy exchanger is a device that can be used to transfer heat and water vapor from one airstream to another (ASHRAE 2020a, Zeng 2017, AHRI 2018). The term "energy exchanger" (also called enthalpy exchanger) is used to emphasize that both sensible energy (if the two airstreams have difference temperatures) and latent energy (if the two airstreams have different vapor pressure) can be recovered. This is in contrast to another term "heat exchanger" which can recover sensible energy only. In comfort applications for buildings, the two airstreams include one outdoor air stream entering from the outside and one exhaust airstream leaving from the inside of a building (see Figure 1). The outdoor air is supplied for ventilation purpose and it usually needs to be conditioned (heated and humidified in winter and cooled and dehumidified in summer) while the exhaust airstream is conditioned and used air leaving from buildings. By transferring energy between the exhaust air and the outdoor air, air-to-air energy recovery has the potential to significantly reduce the energy consumed to condition the outdoor air. It also enables the downsizing of cooling and heating equipment, resulting in capital cost reduction.

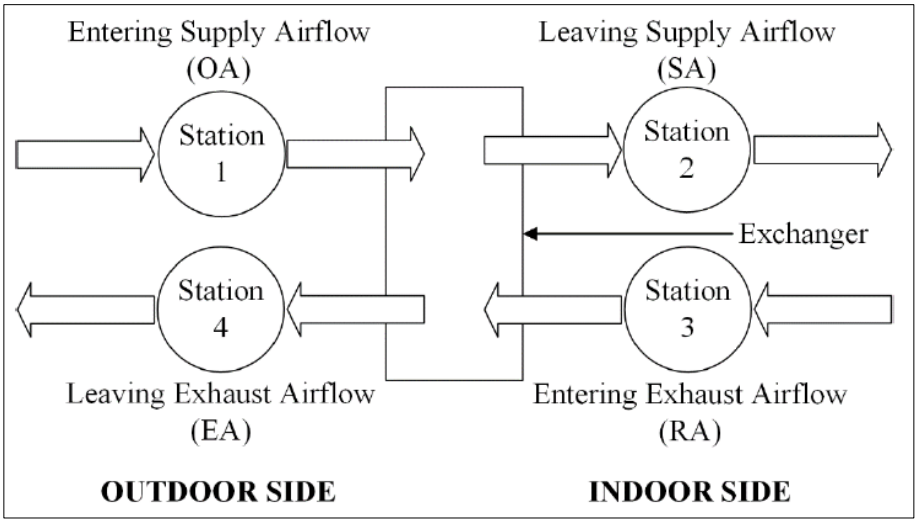

Figure 1: Diagram of airflows across heat exchangers (acquired from AHRI 2018)

Using energy recovery is a requirement of many energy standards and codes, such as ASHRAE Standard 90.1 (ASHRAE 2019b) and the International Green Construction Code (ICC, 2018). For example, Table 1 lists the exhaust air energy requirements for ventilation systems operating less than 8000 hours per year. The requirements are even more stringent for ventilation systems operating more than 8000 hours per year. Though there are some exceptions to the requirements listed in Table 1, the scope of energy recovery requirement has been expanded substantially relative to the pre-2010 versions of ASHRAE Standard 90.1. In particular, the ever-increasing application of dedicated outdoor air systems (DOASs) in the field spurs the use of exhaust air energy recovery further because the central location of outdoor air supply of DOAS facilitates the implementation of energy recovery.

Table 1: Exhaust air energy requirements for ventilation systems operating less than 8000 hours per year

Climate Zone	% Outdoor Air at Full Design Airflow Rate							
	≥10% and <20%	**≥20% and <30%**	**≥30% and <40%**	**≥40% and <50%**	**≥50% and <60%**	**≥60% and <70%**	**≥70% and <80%**	**≥80%**
	Design Supply Fan Airflow Rate (m^3/s)							
3B, 3C, 4B, 4C, 5B	NR	NR	NR	NR	NR	NR	NR	NR
0B, 1B, 2B, 5C	NR	NR	NR	NR	≥12.27	≥5.66	≥2.36	≥1.89
6B	≥13.21	≥12.51	≥5.19	≥2.60	≥2.12	≥1.65	≥1.18	≥0.71
0A, 1A, 2A, 3A, 4A, 5A, 6A	≥12.27	≥7.55	≥2.60	≥2.12	≥1.65	≥0.94	≥0.47	≥0.06
7, 8	≥2.12	≥1.89	≥1.18	≥0.47	≥0.07	≥0.06	≥0.05	≥0.04

Air-to-air energy exchangers can be constructed and operated differently. There are three major types of air-to-air energy exchangers: fixed-plate exchangers, regenerative exchangers, and exchangers with intermediate heat transfer medium circulated in a closed-loop. These exchanger types are briefly described below.

A plate exchanger has multiple alternate airflow channels formed by thin plates to shape the flow channels; the plates may be smooth or have grooves. Plate exchangers are available in many configurations, materials, and airflow patterns (i.e., crossflow, parallel flow, and counterflow (ASHRAE 2020a, Zeng 2017, AHRI 2018). Plates are typically made from plastic and provide sensible heat recovery only (no moisture recovery). However, if plates are made from water vapor permeable materials such as cellulose, polymers and other synthetic materials, total energy (both sensible and latent) exchange can be realized between the two airstreams. Fixed-plate heat exchangers can achieve sensible heat transfer effectiveness between 50% to 80% (Zeng 2017). One advantage of plate exchangers lies in its being a static device and thereby having little or no leakage between the two airstreams.

A regenerative air-to-air energy exchanger uses an energy transfer medium exposed alternatively to the supply and exhaust airstreams to recover energy. The heat and moisture from one airstream are transferred to and stored in the energy transfer media first. The stored energy is then released to another airstream that passes the same channels in the transfer media. Meanwhile, the energy transfer media is regenerated to be capable of storing heat and moisture again when the media is exposed to the first airstream. Regenerative exchangers have two types: rotary and fixed bed. A rotary air-to-air energy exchanger, also called rotary wheel, has a revolving cylinder (wheel) with numerous small airflow channels. The cross-sectional shape of airflow channels can be hexagonal, sinusoidal, or other. If the wheel is for sensible heat recovery (i.e., sensible or heat wheel), the channel structure is usually made from aluminum or stainless steel that works as the heat transfer media. However, if the wheel is used to recover both sensible heat and moisture (i.e., enthalpy or energy wheel), the media surface needs to be coated with a desiccant material such as zeolites, molecular sieves, and silica gels. A fixed-bed regenerator has one or more stationary matrices of storage medium, which are either charged with energy from or discharged to alternating flows of the supply and exhaust air. In contrast to rotary wheels that rely on wheel rotation to alternatively expose the heat transfer media to the two airstreams of fixed flow paths, fixed-bed regenerators rely on dampers to alter the airflow paths through stationary heat transfer media. Rotary wheels are far more well studied and commonly used for energy recovery in buildings. Regenerative exchangers are good at energy recovery. For example, rotary wheels can achieve 80% or even higher heat exchange effectiveness (Zeng 2017) because of their large surface area of heat transfer media and counterflow arrangement. However, cross contamination between the exhaust to the supply airstreams may be a concern in some applications such as cleaning rooms, laboratories, and healthcare facilities. Cross

contamination in rotary wheels comes from two sources: 1) the bulk air leakage from the exhaust to the supply airstream due to pressure difference; and 2) the carryover due to the air trapped within the wheel matrix (including heat transfer media and air passages) as the matrix rotates from the exhaust to the supply airstream.

There are three types of air-to-air energy exchangers that use intermediate energy transfer medium arranged in a closed-loop circuit: 1) heat pipe exchangers, 2) runaround loops, and 3) thermosiphon exchangers.

A heat pipe exchanger is composed of an array of sealed tubes filled with a refrigerant heat transfer fluid. The tubes are placed with one side (evaporator) in the hot airstream and the other side (condenser) in the cold airstream. On the evaporator side, the liquid refrigerant is vaporized in the warm airstream as it absorbs heat from the warm air. The refrigerant vapor then moves to the condenser side, where the vapor condenses and releases energy to the cold airstream. The condensed refrigerant flows back to the evaporator side by gravity or with the aid of an internal capillary wick structure, completing the closed-loop cycle of evaporation and condensation. Typically, the evaporator and the condenser sides are horizontal, or the evaporator is lower than the condenser. Therefore, heat pipe exchangers can operate passively without no external electrical energy input required. Heat pipe exchangers can recovery sensible heat only. The sensible heat transfer effectiveness depends on the air velocity , the airstream temperatures, the geometry and arrangement of the fins and the tubes, and the refrigerant fluid used (Zeng 2017). The heat transfer effectiveness of heat pipe exchangers can reach up to 75%.

A runaround loop has finned-tube coils placed in the supply exhaust air streams, and the coils are connected in a closed loop by counterflow piping filled with a pump-driven intermediate heat transfer fluid (i.e., water or antifreeze solution). Similar to heat pipe

exchangers, runaround loops can recover sensible heat only. Runaround loops have a couple of distinctive features due to the complete separation of supply and exhaust airstreams. First, cross contamination can be eliminated, which is attractive in critical applications such as hospitals and chemical labs. Second, runaround loops accommodate multiple or remote supply air inlets and exhaust air outlets, which is usually the situation found in building renovation.

Thermosiphon exchangers are sealed systems consisting of an evaporator, a condenser and interconnecting piping filled with an intermediate two-phase working fluid. There are two types of thermosiphon exchangers: a sealed tube and a coil type. The sealed-tube thermosiphon resembles heat pipes but it has no wicks and thus relies on the gravity force only to return condensate to the evaporator. The coil-type thermosiphon resembles runaround loops but it does not require a pump to circulate the fluid that experiences two-phase changes.

2.2 Testing and Rating Standards for Air-to-Air Energy Exchangers

2.2.1 Overview of Relevant Standards

Many standards have been developed to test and rate the performance of air-to-air energy exchangers and packaged air-to-air energy recovery ventilators. A packaged energy recovery ventilator consists of not only energy exchangers but also connective ducts and fans. The connective ducts facilitate attaching the ventilator to other HVAC equipment. The fans are used to overcome the pressure drop due to the installation of energy recovery devices. Representative standards for air-to-air heat exchangers include ASHRAE Standard 84, AHRI Standard 1060, EN 308 (BSI 1997), and Eurovent RS 8/C/001-002 (Eurovent 2019) while representative standards for packaged energy recovery ventilators include ISO 16494 (ISO 2014) and CSA C439 (CSA 2018). Considering the focus of this research, only standards for air-to-air energy exchangers are briefly reviewed in this section.

As Table 2 shows, the standards for air-to-air energy exchangers are used for either product performance testing or product performance rating. ASHRAE Standard 84 and EN 308 are testing standards and they define the methods and procedures to measure the performance of air-to-air energy exchangers. AHRI 1060 and Eurovent RS 8/C/001 & 002 are rating standards that provide conditions and procedures for rating and certifying the performance of air-to-air energy exchangers. Certainly, a rating standard must define its own or refer to another testing standard to specify the test requirements for performance rating. In this respect, AHRI 1060 is based on ASHRAE Standard 84 while Eurovent RS 8/C/001 & 002 are based on EN 308

Both ASHRAE Standard 84 and EN 308 have a strong focus on laboratory testing. Though ASHRAE Standard 84 covered the field testing concisely in its earlier versions, its most recent version released in 2020 has relocated the discussion of field testing to an informative appendix. The current version of EN 308 does not cover field testing. However, the next edition of EN 308, currently in development, is intended to include field testing in its scope.

Regarding the exchanger types covered by the standards, ASHRAE Standard 84 and EN 308 cover all exchanger typed discussed in Section 1.1; AHRI Standard 1060 covers fixed plate, heat pipe, and rotary exchangers, but not runaround loop and fixed-bed regenerators; Eurovent RS 8/C/001 and 002 cover fixed-plate and regenerative exchangers.

Table 2: General information of the standards for air-to-air energy exchangers

Item		ASHRAE 84	AHRI 1060	EN 308	Eurovent RS 8/C/001 & 002
Publisher		ASHRAE	AHRI	The European Committee for Standardization	Eurovent Certita Certification
Purpose		Testing	Rating	Testing	Rating
Laboratory test		X	X	X	X
Field test		X	-	-	-
Exchanger Type	Fixed Plate	X	X	X	X
	Regenerative	X	X	X	X
	Runaround	X	-	X	-
	Heat Pipe	X	X	X	-

All the standards in Table 2 evaluate the performance of air-to-air energy based on three aspects: thermal, leakage, and pressure drop. The U.S. Standards (ASHRAE Standard 84 and AHRI 1060) and the European Standards (EN 308 and Eurovent RS 8/C/001-002) have similar concepts and principles in the definition and evaluation of exchanger performance although some subtle differences exist in certain terminology and equations. Because ASHRAE Standard 84 is employed to test commercial energy exchangers in this work, its performance metrics (Table 3), test parameters, conditions to accept test results and uncertainty analysis are presented sequentially in the rest of this section.

Table 3: Performance metrics for air-to-air energy exchangers

Performance Metrics	ASHRAE Standard 84
Thermal	-Sensible, latent, and total effectiveness -Sensible, latent, and total net effectiveness -Recovery efficiency ratio -Enthalpy recovery ratio
Leakage	-Exhaust air transfer ratio (EATR) -Outdoor air correction factor (OACF)
Pressure Drop	-Supply airstream pressure drop -Exhaust airstream pressure drop

2.2.2 ASHRAE Standard 84

ASHRAE Standard 84 uses effectiveness (sensible, latent, and total) as the key metric to evaluate the actual energy transfer rate relative to the thermodynamically possible maximum energy transfer rate at given operating conditions. In the latest version of ASHRAE Standard 84 (ASHRAE 2020a), the sensible, latent, and total effectiveness is determined as follows:

$$\varepsilon_s = \frac{m_2(c_{p,1}T_1 - c_{p,2}T_2)}{m_{min}(c_{p,1}T_1 - c_{p,3}T_3)} \quad (1)$$

$$\varepsilon_l = \frac{m_2(h_{fg,1}W_1 - h_{fg,2}W_2)}{m_{min}(h_{fg,1}W_1 - h_{fg,3}W_3)} \quad (2)$$

$$\varepsilon_t = \frac{m_2(h_1 - h_2)}{m_{min}(h_1 - h_3)} \quad (3)$$

Where, ε_s, ε_l, and ε_t represents the sensible effectiveness, latent effectiveness, and total effectiveness, respectively; T is the air dry-bulb temperature (℃); W is the air humidity ratio; m is the air mass flow rate (kg/s); c_p is the specific heat of dry air (kJ/kg-℃); h_{fg} is the heat of vaporization of water (kJ/kg); h is the specific enthalpy of moist air (kJ/kg); the subscripts 1, 2, and 3 represent the corresponding station number as shown in Figure 1; m_{min} represents the minimum of m_2 and m_3.

If the specific heat of dry air and the heat of vaporization of water are assumed to keep constant at different stations, Equations 4 and 5 can be simplified to the following:

$$\varepsilon_s = \frac{m_2(T_1 - T_2)}{m_{min}(T_1 - T_3)} \quad (4)$$

$$\varepsilon_l = \frac{m_2(W_1 - W_2)}{m_{min}(W_1 - W_3)} \quad (5)$$

ASHRAE Standard 84 defines recovery efficiency ratio as:

$$RER = \frac{m_2|h_1 - h_2|}{P_{ma} + P_{aux}} \quad (6)$$

Where,

h : the enthalpy of air (kJ/kg)

P_{ma}: the power value of moving air for both streams (kW)

P_{aux}: the auxiliary power input to the heat exchanger (kW)

In addition to effectiveness, ASHRAE Standard 84 also defines net effectiveness for energy exchangers. The net effectiveness (sensible, latent, and total) is calculated similar to the corresponding effectiveness but account for the portion of the psychrometric change in the leaving supply airflow (Station 2 in Figure 1) that is the result of leakage from the entering exhaust airflow (Station 3 in Figure 1). Details on the equations for net effectiveness can be found in ASHRAE (2020a).

Exhaust air transfer ratio (EATR) and outdoor air correction factor (OCAF) are the two metrics used by ASHRAE Standard 84 to evaluate the leakage of air-to-air energy exchangers. Tracer gas tests, with the tracer gas injected at Station 3, are used to determine EATR and OACF. The equations for EATR and OACF are expressed as follows:

$$EATR = \frac{\sigma_2 - \sigma_1}{\sigma_3 - \sigma_1} * 100\% \quad (7)$$

$$OACF = \frac{m_1}{m_2} \quad (8)$$

Where, σ_n is the tracer gas concentration at each indicated station n

The air friction pressure drop through the exchanger is determined for both supply and exhaust airstreams:

$$\Delta p_s = P_{s,1} - P_{s,2}$$

$$\Delta p_e = P_{s,3} - P_{s,4}$$

Where, Δp_s and Δp_e represent the pressure drop (Pa) respectively for the supply airs and exhaust air, P_s is the air static pressure (Pa), and the subscripts 1-4 represent the station number as shown in Figure 1.

ASHRAE Standard 84 specifies that a number of inequalities must be checked to determine whether the test data are accepted. These inequalities are defined to ensure the operating conditions (i.e., the entering supply air dry-bulb temperature and humidity ratio) and the mass and energy balances are maintained during the laboratory testing. For the tests on effectiveness, the following inequalities need to be checked and satisfied:

$$\frac{|\delta T_1|}{|T_1 - T_3|} < 0.02 \quad (9)$$

$$\frac{|\delta T_3|}{|T_1 - T_3|} < 0.02 \quad (10)$$

$$\frac{|\delta W_1|}{|W_1 - W_3|} \begin{cases} < 0.05 & (if\ W_1 > W_3) \\ < 0.1 & (if\ W_1 < W_3) \end{cases} \quad (11)$$

$$\frac{|\delta W_3|}{|W_1 - W_3|} \begin{cases} < 0.05 & (if\ W_1 > W_3) \\ < 0.1 & (if\ W_1 < W_3) \end{cases} \quad (12)$$

$$\frac{|m_1 + m_3 - m_2 - m_4|}{m_{\min\,(1,3)}} < 0.05 \quad (13)$$

$$\frac{|m_1 W_1 + m_3 W_3 - m_2 W_2 - m_4 W_4|}{m_{\min\,(1,3)} |W_1 - W_3|} < 0.2 \qquad (14)$$

$$\frac{|m_1 h_1 + m_3 h_3 - m_2 h_2 - m_4 h_4|}{m_{\min\,(1,3)} |h_1 - h_3|} < 0.2 \qquad (15)$$

Where, δT and δW are the maximum deviation of measured temperature and humidity ratio from their corresponding mean value over the testing period.

Of the above equations, Equations 9 and 10 are the inequality checks for inlet air temperature; Equations 11 and 12 are for inlet air humidity ratio; Equation 13 is for the dry airflow mass balance; Equation 14 is for the water vapor mass balance; and Equation 15 is for the moist air energy balance. It needs to be noted that Equation 15 applies only when no condensate or frosting occurs; otherwise, the condensate or the storage of water in the exchanger due to frost formation needs to be considered, which is not simple.

For leakage tests, the dry air mass balance (Equation 15) needs to be checked and satisfied. In addition, the following inequality needs to checked for tracer gas mass balance:

$$\frac{|m_1 \sigma_1 + m_3 \sigma_3 - m_2 \sigma_2 - m_4 \sigma_4|}{m_{\min\,(1,3)} |\sigma_1 - \sigma_3|} < 0.15 \qquad (16)$$

Laboratory tests of air-to-air energy exchangers require a number of instruments to measure temperature, pressure, flow rate, and concentration. Therefore, instrumental bias and precision affect the accuracy of the test results. ASHRAE Standard 84 specifies the upper limits of results uncertainty. Here, uncertainty expresses the difference between measured performance and the true value of a measured quantity. Table 4 lists the uncertainty limits for different measured performance results.

Table 4: Uncertainty limits of measured performance results

Uncertainties	ASHRAE 84
$U(\varepsilon_s)$	5%
$U(\varepsilon_l)$	7%
$U(\varepsilon_t)$	$\frac{\lvert\varepsilon_l-\varepsilon_t\rvert 5\%+\lvert\varepsilon_s-\varepsilon_t\rvert 7\%}{\lvert\varepsilon_l-\varepsilon_s\rvert}$
$U(\Delta p_s)$	$0.1 * \Delta p_s$
$U(\Delta p_e)$	$0.1 * \Delta p_e$
$U(EATR)$	3%
$U(OACF)$	0.02

2.2.3 AHRI Standard 1060

AHRI Standard 1060 is an industry-established standard for rating air-to-air energy exchangers. This standard is based on ASHRAE Standard 84 and specifies the testing requirements, rating requirements, minimum data requirements for published ratings, marking and nameplate data, and conformance conditions.

Before 2020, AHRI Standard 1060 required the thermal performance rating (i.e., sensible, latent, and total effectiveness) be based on the tests at two balanced airflow rates (i.e., 100% and 75% of the rated airflow rate) and standard winter and summer conditions as listed in Table 5.

Table 5: Test conditions in winter & summer

Test Condition	Entering Supply Air		Entering Exhaust Air	
	Dry-bulb temperature (°C)	Wet-bulb temperature (°C)	Dry-bulb temperature (°C)	Wet-bulb temperature (°C)
Winter	1.7	0.6	21.1	14.4
Summer	35	25.6	23.9	17.2

As of 2020, AHRI requires the use of laboratory tests to verify ratings generated by the energy exchanger manufacturer's software. Instead of using standard winter and summer conditions, the thermal performance rating is based on a broad psychrometric range as shown in Figure 2.

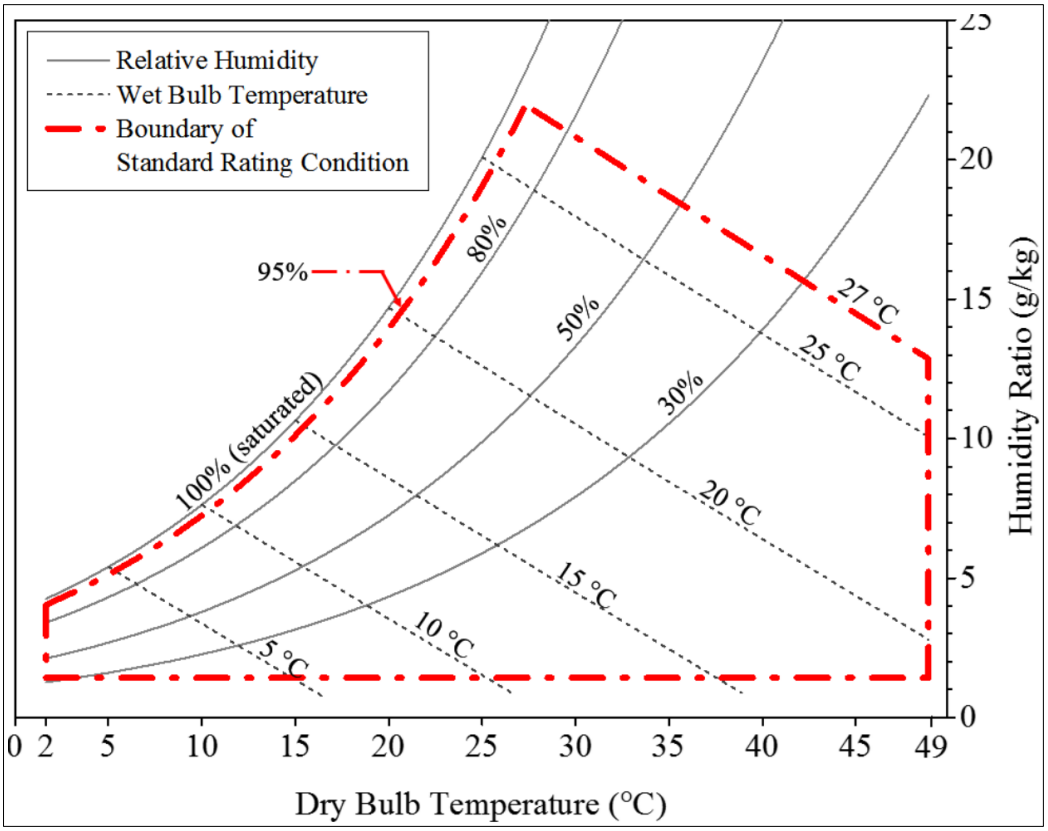

Figure 2: Illustration of range of standard rating conditions (acquired from AHRI 2018)

In addition to the psychrometric range of entering supply air and exhaust air conditions, the current AHRI standard also specifies the ranges of airflow and pressure differential used for thermal performance rating as follows:

- The entering supply air and exhaust air flow rates are in the range of the minimum and maximum declared by the manufacturer.
- The supply flow ratio, defined as the volumetric air flow rate at Station 2 divided by that at Station 3, ranges between 0.5 and 2.0.
- The pressure differential, defined as the static pressure at Station 2 minus that at Station 3, is zero.

The test conditions towards leakage rating (i.e., EATR and OACF) include the following:

- Entering air (both supply and exhausts) is at laboratory ambient conditions.
- The entering air flow rates are in the range of the minimum and maximum declared by the manufacturer.
- The supply flow ratio ranges between 0.5 and 2.0.
- The pressure differential ranges between -1250 Pa and 1250 Pa.

AHRI Standard 1060 requires measurements are taken for 30 minutes after a period of 30 minutes with stable input conditions.

2.3 Extrapolation of Test Performance Data

Testing air-to-air energy exchangers in laboratories is expensive. Therefore, laboratory tests are performed at a limited number of operating conditions for selected products. These laboratory tests have the main purposes of product performance rating and validation of manufacture's software for product performance prediction. In reality, exchangers can run in a wide range of operating conditions that may vary in entering air properties (temperature and humidity ratio), airflow rates, supply flow ratio, and pressure differential. In addition, energy exchanger manufacturers make many different sizes of products. Some large products may be too big to be handled in laboratories. For example, Figure 3 shows the nominal air flow rate ranges of commercial enthalpy wheels of different brands. This figure indicates that a large number of commercial enthalpy wheels have their nominal air flow rates more than 2.12 m^3/s, which is the upper limit that the leading independent test facilities (i.e., the Intertek Lab in Cortland, NY and the Lucerne HVAC Testing Laboratory in Switzerland) can accommodate. Therefore, there is a need for extrapolation of test performance data. Existing extrapolation approaches are reviewed in this subsection.

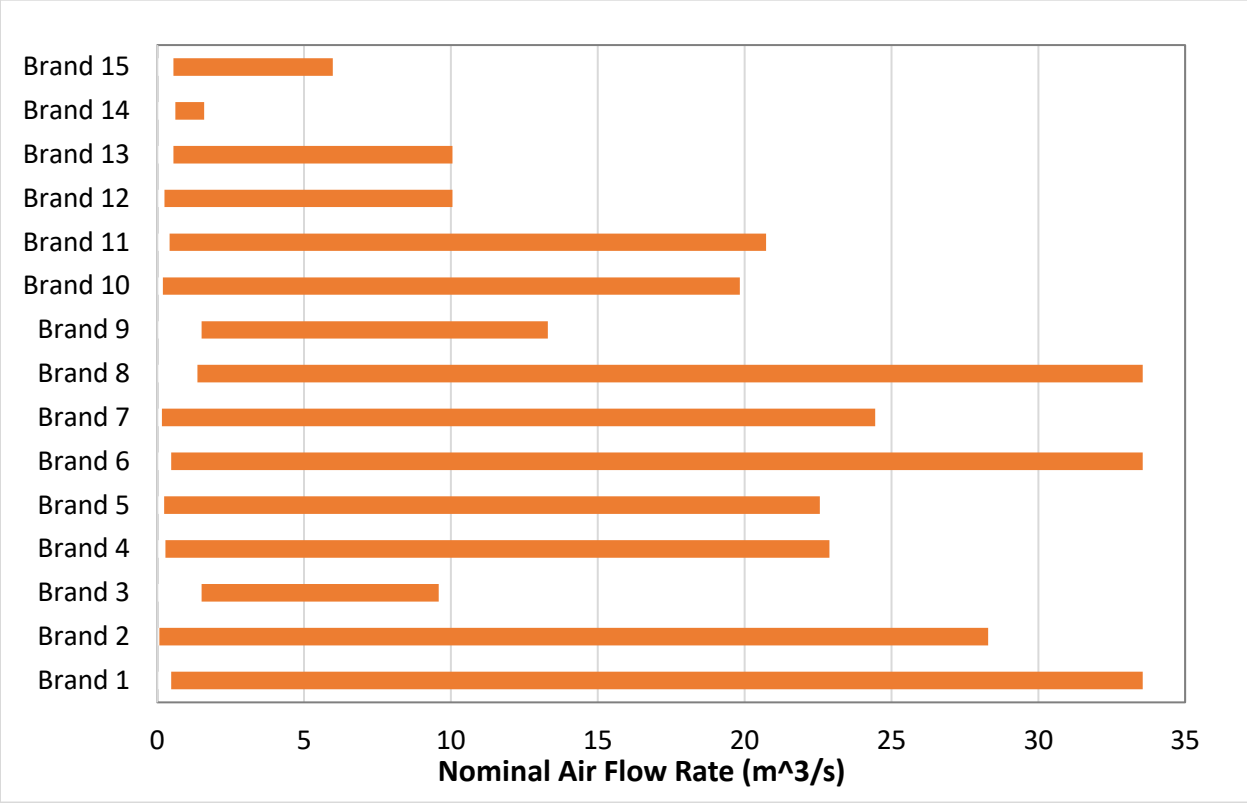

Figure 3: Nominal air flow rates for different commercial brands

2.3.1 Extrapolation from Small to Large Sizes

AHRI Standard 1060 allows energy exchangers with nominal air flow rate larger than 2.4 m^3/s (5000 scfm) to be rated the same as the smaller ones as long as they are in the same Basic Model Group. Unfortunately, the Basic Model Group is not clearly defined in AHRI Standard 1060 (AHRI 2018) and its Operations Manual (AHRI 2020). Instead of using Basic Model Group, Technical Similarity Group (TSG) is used in this work and it is defined with the assistance from the Project Monitoring Subcommittee (PMS) of ASHRE RP-1799.

For rotary regenerative energy exchangers, products of the same TSG need to have the following identical characteristics (see Figure 4):

- Flow configuration (i.e., counter flow)
- Matrix geometry (shape, hydraulic diameter dh)

- Matrix structure (material, thickness δ1)
- Desiccant (material, thickness δ2)
- Wheel depth (L)

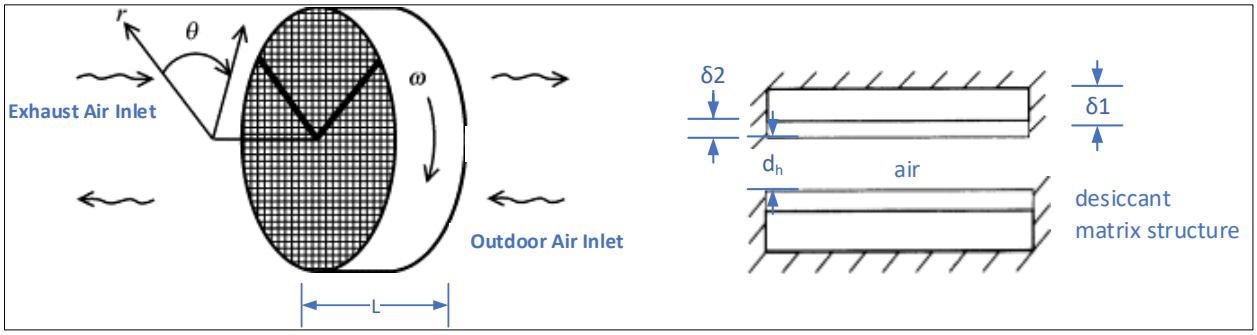

Figure 4: Rotary regenerative energy exchanger geometry: exchanger dimension (left) and air channel dimension (right) (Modified from Simonson and Besant 1999)

Based on the AHRI approach of extrapolation, rotary regenerative exchangers of the same TSG have the same rated performance at the same wheel rotation speed and the air flow rate leading to the same face velocity at each airstream. Although the AHRI approach has been used to extrapolate rating tests of small exchangers to larger exchangers, its validity has never been investigated and established in open technical literature.

2.3.2 Extrapolation from Test Conditions to Real Operating Conditions

Stiesch et al. (1994) developed a model that estimates the performance of energy wheels as a function of the wheel rotation speed and inlet air conditions. The model was implemented in TRNSYS to perform annual regenerator performance simulations. This model, however, did not consider humidity effects and could not provide a physical insight on why the effectiveness changes with different inlet operating conditions.

Freund et al. (2003) proposed a simple model to predict the energy wheel effectiveness. The model was based on the classical ε-NTU method for standard counter flow heat exchangers.

Based on the assumption that an energy wheel, if operated at high rotation speed, would have perform similarly as a counter flow heat exchanger, Freund et al. estimated the sensible and latent effectiveness of an energy wheel by multiplying a correction factor they developed by the effectiveness values of an equivalent counter flow heat exchanger.

Simonson (1998) have developed a numerical model for energy wheels to predict heat and moisture transfer during sorption, condensation, and frosting processes. The sensible, latent, and total effectiveness can be predicted for different energy wheel designs. In addition, the numerical model is utilized to examine the impact of multiple factors such as the phase change, rotation speed, heat conduction in the matrix, extrapolation of experimental test data, and the effect of operating conditions. The numerical model was validated with laboratory and field experiments covering a range of mass flow rates, temperature, and humidity.

Simonson and Besant (1999) derived and developed dimensionless groups for energy wheels to reduce the dimensions of input variables. The dimensionless groups include:

- NTU_o: Overall number of transfer units
- Cr_o*: Overall matrix heat (or moisture) capacity ratio
- Crm_o*: Overall matrix moisture capacity ratio
- $Cr^*_{mt,o}$: The storage of moisture in the desiccant
- H*: Refers to the ratio of latent to sensible energy differences between the supply air and exhaust air

Based on the dimensionless groups, the following correlation equations were developed to calculate the effectiveness of rotary energy exchangers:

$$\varepsilon_S = \frac{NTU_\circ}{1+NTU_\circ}\left(1-\frac{1}{7.5Cr_\circ^*}\right) - \left[\frac{0.26\left(\frac{Cr_\circ^*}{Wm^2 Crm_\circ^*}\right)^{0.28}}{7.2\left(Cr_\circ^*\right)^{1.53}+\frac{210}{\left(NTU_\circ\right)^{2.9}}-5.2} + \frac{0.31\eta}{(NTU_\circ)^{0.68}}\right]H^* \qquad (17)$$

$$\varepsilon_l = \frac{NTU_\circ}{1+NTU_\circ}\left(1-\frac{1}{0.54\left(Cr_{mt,o}^*\right)^{0.86}}\right)\times\left(1-\frac{1}{(NTU_\circ)^{0.51}\left(Cr_{mt,o}^*\right)^{0.54}H^*}\right) \qquad (18)$$

$$\varepsilon_t = \frac{\varepsilon_s+\varepsilon_1 H^*}{1+H^*} \qquad (19)$$

Simonson and Besant's effectiveness correlation equations are based on a solid and experimentally validated numerical model for rotary energy exchangers. However, these equations need geometrical and material properties that may not be easily obtained. To address this problem, Jeong and Mumma (2005) developed correlations that only rely on entering air properties (e.g., temperature, relative humidity, face velocity and ratio of airflow rate). Based on typical energy wheel construction and operating parameters (e.g., a wheel depth of 0.2 m, a wheel rotation speed of 20 rpm, a 0.07-mm aluminum matrix structure, and sinusoidal air channels of 1.5 mm height and 3 mm width), the numerical model from Simonson and Besant were run many times based on a 2^k factorial experiment design method, where the superscript k refers to the total number of independent variables (k=6). The six independent variables include air face velocity, outdoor air temperature, outdoor air relative humidity, exhaust air temperature, exhaust air relative humidity, and the ratio of airflow rate between the two airstreams. Two sets of first-order linear regression equations were developed for rotary energy wheels with different desiccant materials: one for wheels with silica gel and another for wheels with molecular sieve. For example, the correlations for energy wheels with molecular sieve took the following forms:

$$\varepsilon_s=(\alpha_0+\alpha_1(V_{si})+\alpha_2(T_{si})+\alpha_3(\emptyset_{si})+\alpha_4(Q_R)+\alpha_5(V_{si*}T_{si})+\alpha_6(V_{si*}\emptyset_{si})+\alpha_7(V_{si*}Q_R)+\alpha_8(T_{si*}\emptyset_{si})+$$
$$\alpha_9(T_{si*}Q_R)+\alpha_{10}(\emptyset_{si*}Q_R)+\alpha_{11}(V_{si*}T_{si*}\emptyset_{si})+\alpha_{12}(V_{si*}T_{si*}Q_R)+\alpha_{13}(T_{si*}\emptyset_{si*}Q_R)) \qquad (20)$$

$$\varepsilon_1=\beta_0+\beta_1(V_{si})+\beta_2(T_{si})+\beta_3(T_{ei})+\beta_4(\emptyset_{si})+\beta_5(\emptyset_{ei})+\beta_6(Q_R)+\beta_7(V_{si}*T_{si})+\beta_8(V_{si}*T_{ei})+\beta_9(V_{si}*\emptyset_{si})+\beta_{10}(V_{si}*\emptyset_{ei})+\beta_{11}(V_{si}*Q_R)+\beta_{12}(T_{si}*T_{ei})+\beta_{13}(T_{si}*\emptyset_{si})+\beta_{14}(T_{si}*\emptyset_{ei})+\beta_{15}(T_{si}*Q_R)+\beta_{16}(T_{ei}*\emptyset_{si})+\beta_{17}(T_{ei}*\emptyset_{ei})+\beta_{18}(\emptyset_{si}*\emptyset_{ei})+\beta_{19}(V_{si}*T_{si}*T_{ei})+\beta_{20}(V_{si}*T_{si}*\emptyset_{ei})+\beta_{21}(V_{si}*T_{si}*Q_R)+\beta_{22}(V_{si}*T_{ei}*\emptyset_{ei})+\beta_{23}(V_{si}*\emptyset_{si}*\emptyset_{ei})+\beta_{24}(T_{si}*T_{ei}*\emptyset_{si})+\beta_{25}(T_{si}*T_{ei}*\emptyset_{ei})+\beta_{26}(T_{si}*\emptyset_{si}*\emptyset_{ei})+\beta_{27}(T_{ei}*\emptyset_{si}*\emptyset_{ei})+\beta_{28}(V_{si}*T_{si}*T_{ei}*\emptyset_{ei})+\beta_{29}(T_{si}*T_{ei}*\emptyset_{si}*\emptyset_{ei}) \quad (21)$$

Where,

V_{fi}: face velocity (m/s)

T_{si}: outdoor air temperature (°C)

ϕ_{si}: outdoor relative humidity (a numerical value between 0 and 1)

T_{ei}: exhaust air temperature (°C)

ϕ_{ei}: exhaust relative humidity (a numerical value between 0 and 1)

Q_r: exhaust-air to outdoor-air flow ratio (a numerical value between 0 and 1)

α and β: coefficients are calculated and provided by Jeong and Mumma (2005) with their values shown in Tables 6 and 7:

Table 6: Values for coefficient α

Coefficient	Value	Coefficient	Value
α_0	1.05319	α_7	-0.0325
α_1	-0.022312	α_8	-0.00132813
α_2	0.00124609	α_9	-0.00232188
α_3	0.005	α_{10}	-0.01
α_4	-0.032	α_{11}	-0.00126562
α_5	0.000117969	α_{12}	0.000453125
α_6	0.0025	α_{13}	0.003625

Table 7: Values for coefficient β

Coefficient	Value	Coefficient	Value	Coefficient	Value
β_0	1.18598	β_{10}	-0.012417	β_{20}	0.008125
β_1	-0.026498	β_{11}	-0.031875	β_{21}	0.00234375
β_2	-0.022742	β_{12}	0.00119604	β_{22}	-0.00291667
β_3	-0.009825	β_{13}	0.047533	β_{23}	0.215
β_4	-0.11275	β_{14}	0.059808	β_{24}	-0.00231667
β_5	-0.18408	β_{15}	-0.00596875	β_{25}	-0.00280417
β_6	-0.030625	β_{16}	0.014	β_{26}	-0.11533
β_7	-0.00382031	β_{17}	0.017417	β_{27}	-0.023333
β_8	0.00195833	β_{18}	0.081667	β_{28}	-0.0005625
β_9	-0.11775	β_{19}	0.000134375	β_{29}	0.00566667

2.4 Air-to-Air Energy Recovery in Building Energy Simulations

Building energy simulation programs calculate thermal loads, HVAC system responses to thermal loads, and resulting energy consumption based on the principles of heat transfer, energy balance, and empirical equations for equipment performance. A comprehensive energy simulation program normally needs detailed inputs such as building geometry, construction

materials, internal loads (e.g., profiles of occupants, lighting, and miscellaneous energy loads), HVAC equipment, and system configurations. Many building performance simulation programs provide multifaceted functionalities such as equipment sizing, energy estimation, thermal comfort analysis, and air flow analysis. There exist a large number of building energy simulation programs, which may vary in different aspects, such as modeling features and capabilities, ease of use, validation effort, and source availability (Crawley et al. 2008).

As a widely used energy efficiency technology, air-to-air energy recovery modeling is supported by many energy simulation programs. Therefore, many studies are available in literature using simulation programs to investigate the benefits of energy recovery in building design. Some of them are reviewed below.

Liu et al. (2010) used EnergyPlus to investigate the energy savings of using energy recovery ventilator (ERV) in a residential building with different climatic conditions, enthalpy efficiency, fresh air change rate, and fan power consumption of ERV. Zhou et al. (2007) used EnergyPlus to study the energy performance of ERV with different indoor temperature setpoints in Shanghai and Beijing, China. They found that ERV operation in cold climate (Beijing) was uneconomical when the cooling set-point was above 24 C. Jiru (2014) used prototype commercial building models developed in EnergyPlus to estimate the energy savings from the combination of energy conservation measures, including air-to-air energy recovery. In the series of Advanced Energy Design Guides, air-to-air energy recovery was included in the recommended design package for several different commercial building types. The recommendation was made based on EnergyPlus simulations (e.g., Thornton et al. 2009).

In addition to EnergyPlus, TRNSYS is another software that has been used in many simulation studies with air-to-air energy recovery. For example, Al-Hyari and Kassai (2021)

applied TRNSYS software to evaluate the benefits of adding ERV to a variable refrigerant flow air-conditioning system. Rasouli et al. (2010) used TRNSYS to investigate the annual energy savings with the use of ERVs for a practical range of sensible and latent effectiveness. The impact of ERV on annual cooling and heating energy consumption was investigated by modeling a 10-storey office building in four cities in the U.S. with different climates.

Chapter 3: Selected Exchangers and Testing Conditions

This chapter includes three sections. Section 3.1 covers the two sets of enthalpy wheels selected for testing. Each wheel set consists of three different sizes with the same design and construction satisfying the TSG requirement. Section 3.2 provides a brief description of the laboratory testing facility at Intertek, where the two set of wheels were tested. Section 3.3 presents the test conditions including the number of tests, the entering air temperature and humidity, the wheel rotation speed, the air flow rate, and the air face velocity.

3.1 Exchangers Selected for Testing

Two sets of air-to-air energy wheels from different manufacturers were selected for laboratory testing. Each set includes three wheels of different sizes (i.e., small, medium, and large). Efforts were taken while selecting the wheels to ensure the large wheel is about twice bigger than the medium one, which is twice bigger than the small one. Table 8 shows the dimensions of the two sets of wheels. The wheel face area listed in the table refers to the net face area excluding the hub, the banding, and the beams and spokes for structural support. The three wheels in each set have the same major technical specifications, which are:

- desiccant material
- matrix support material
- heat transfer surface area density
- porosity
- air channel geometry
- not using purge sections

Therefore, if the same rotation speed and the same air face velocity are applied during the laboratory tests, the wheels of each set meet the criteria of the same Technical Similarity Group (TSG), as described in Section 2.3.1.

Table 8: Overview of the tested energy wheels

Set	Size	Desiccant	Wheel depth (cm)	Wheel diameter (cm)	Wheel face area (m^2)
W1	small	silica gel	7.62	63.5	0.293
	medium	silica gel	7.62	91.44	0.549
	large	silica gel	7.62	132.08	1.225
W2	small	molecular sieve	20	60	0.225
	medium	molecular sieve	20	90	0.545
	large	molecular sieve	20	130	1.157

3.2: Testing Facility

All tests took place at Intertek in its highly automated and instrumented facility for ERV testing. For many years, the testing facility has been an AHRI approved and certified facility for testing ERVs according to standards AHRI 1060 and ASHRAE 84. The facility operates on an open-loop four-blower push/pull reconditioning and control system, allowing for precise airflow and pressure control. National Lab Instruments LabVIEW software is used to obtain and plot real-time data, test conditions, and control parameters at 5-second intervals. Prior to testing, Intertek needs to 1) install ductwork and connect the tested energy exchanger with the test facility control loops; and 2) check pressure and airflow to ensure no leakage. Figure 5 illustrates the laboratory facility setup along with measurement locations. All four stations use flow nozzles to measure the volumetric airflow rate. Each nozzle station is comprised of a discharge chamber and a receiving chamber separated by a partition in which different nozzles are located. Air dry-bulb temperature, wet-bulb temperature, pressure, and tracer gas concentration are measured at

each station prior to air entering and leaving the energy exchanger. Table 9 shows the instrumental accuracies that are used to calculate the test uncertainties.

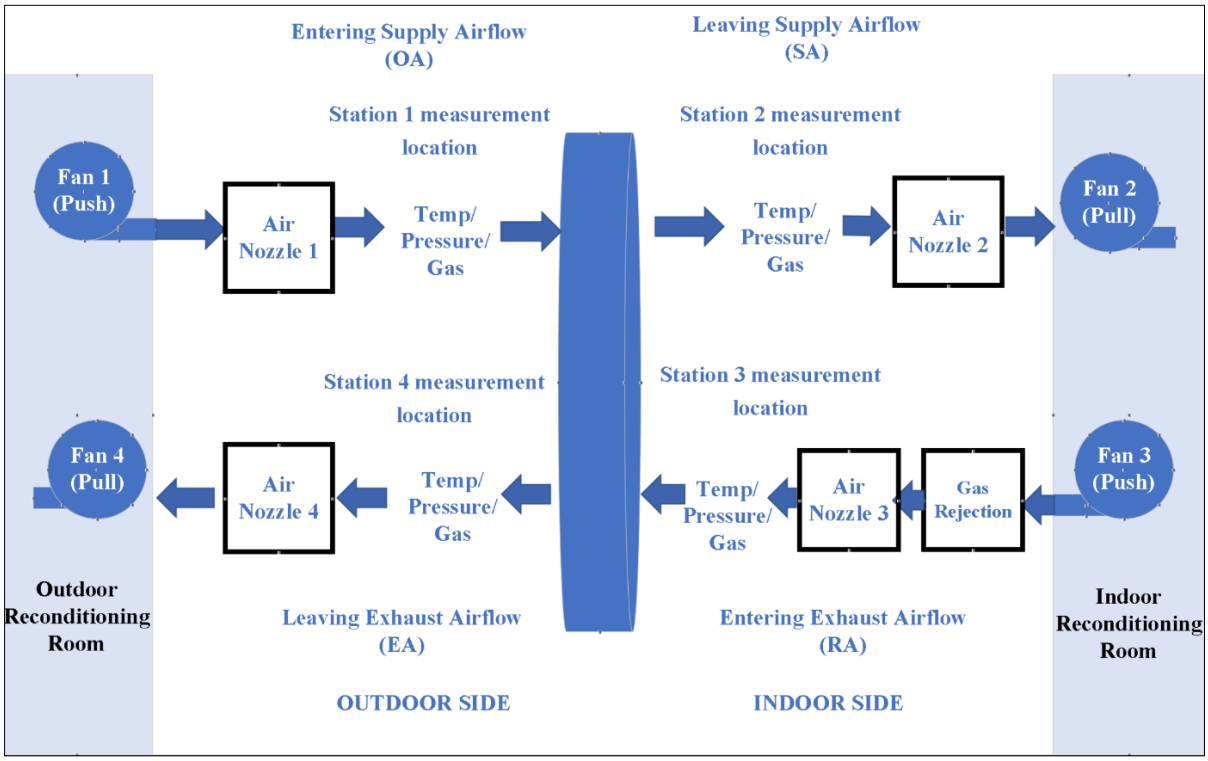

Figure 5: Intertek's open-loop design along with measurement locations

Table 9: Accuracy of the instruments used in the testing facility

Instrument	Accuracy	Unit
Dry-bulb temperature	0.0028	°C
Wet-bulb temperature	0.056	°C
Pressure	2.5	Pa
Delta pressure (nozzle)	2.5	Pa
Nozzle diameter	0.0051	cm

3.3 Test Conditions

Table 10 shows the laboratory tests as well as the applicable psychrometric conditions for all tested energy exchangers. The large wheels have seven effectiveness tests, three of which are used for the small- and medium-size wheels. Each wheel has two tracer gas tests.

Table 10: Laboratory test conditions on inlet air temperature and pressure differential

Size	Test No.	Test Type	Outdoor Air DB Temp (ºC)	Outdoor Air WB Temp (ºC)	Exhaust Air DB Temp (ºC)	Exhaust Air WB Temp (ºC)	Pressure differential (Pa)
Large	1	Effectiveness	37.8	26.7	21.1	15.6	0
	2	Effectiveness	32.2	23.9	21.1	15.6	0
	3	Effectiveness	37.8	26.7	21.1	15.6	0
	4	Effectiveness	37.8	28.3	23.9	18.3	0
	5	Effectiveness	37.8	23.3	21.1	14.4	0
	6	Effectiveness	26.7	20.0	20.0	14.4	0
	7	Effectiveness	23.9	21.1	18.3	14.4	0
	8	Tracer gas	Ambient	Ambient	Ambient	Ambient	0
	9	Tracer gas	Ambient	Ambient	Ambient	Ambient	-500
Medium	1	Effectiveness	37.8	26.7	21.1	15.6	0
	2	Effectiveness	32.2	23.9	21.1	15.6	0
	3	Effectiveness	37.8	26.7	21.1	15.6	0
	4	Tracer gas	Ambient	Ambient	Ambient	Ambient	0
	5	Tracer gas	Ambient	Ambient	Ambient	Ambient	-500
Small	1	Effectiveness	37.8	26.7	21.1	15.6	0
	2	Effectiveness	32.2	23.9	21.1	15.6	0
	3	Effectiveness	37.8	26.7	21.1	15.6	0
	4	Tracer gas	Ambient	Ambient	Ambient	Ambient	0
	5	Tracer gas	Ambient	Ambient	Ambient	Ambient	-500

It is worth mentioning the following for Table 10:

- The large wheels have seven effectiveness tests, the purpose of which is to cover a wide range of moist air properties of the two airstreams and understand the extent of operating conditions on the effectiveness of energy exchangers.

- The small and medium wheels have three effectiveness tests similar to the first three test conditions of the large wheels. The purpose of having three different test conditions for all wheels is to validate the approach used by AHRI Standard 1060 to extrapolate the effectiveness of energy exchangers of the same TSG from small to large sizes.
- Test 3 is different from the other effectiveness tests by having a different face velocity. The purpose is to investigate the impact of air face velocity on the effectiveness of energy exchangers by comparing the results between Test 1 and Test 3.
- All wheels have two tracer gas tests with different pressure differentials between the leaving supply air (P_2) and the entering exhaust air (P_3). The purpose of these two tests is to validate the approach used by AHRI Standard 1060 to extrapolate the EATR and the OACF of energy exchangers of the same TSG from small to large sizes.

In addition to the psychrometric conditions of supply air and exhaust air and the pressure differential between Station 2 and Station 3, the laboratory test conditions also include the specification of airflow rate and the rotational speed. Table 11 shows the airflow rates, air face velocities, wheel rotational speeds for all tests.

Regarding the airflow rate and the air face velocity, the following needs to be noted:

- For the first set of three wheels (labelled as W1 in Table 11), the air face velocity was set at 3.048 m/s for all tests except Test 3 which had a 1.829 m/s face velocity. Test 3 had 60% of the airflow used in other tests.
- For the second set of three wheels (labelled as W2 in Table 11), the air face velocity was set at 3.302 m/s for all tests except Test 3 which had a 2.311 m/s face velocity. Test 3 had 70% of the airflow used in other tests. This setting was different from the original plan of having 60% of the full flow for Test 3. The major reason of the above change was mainly

due to the laboratory facility limitations and this change had no impact on this project's research outcomes.

Table 11: Laboratory test conditions on airflow rate, air face velocity and wheel speed

Energy exchanger	Test	Airflow rate (m^3/s)	Air face velocity (m/s)	Wheel speed (rpm)
W1-small	All tests except Test 3	0.446	3.048	79
	Test 3	0.267	1.829	
W1-medium	All tests except Test 3	0.883	3.048	74
	Test 3	0.530	1.829	
W1-large	All tests except Test 3	1.868	3.048	74
	Test 3	1.121	1.829	
W2-small	All tests except Test 3	0.371	3.302	21
	Test 3	0.260	2.311	
W2-medium	All tests except Test 3	0.900	3.302	22
	Test 3	0.630	2.311	
W2-large	All tests except Test 3	1.910	3.302	21
	Test 3	1.337	2.311	

Ideally, the rotational speed should be kept exactly the same for the same set of wheels. However, there are slight differences in actual tests from what the manufacturers have declared. The reasons are explained below.

For the first set of wheels, the large one was tested first and its rotational speed was measured at 74 rpm. In contrast, the manufacturer declared that the rotational speed would be 50 rpm if the motor was run at the rated voltage. After observing the rpm difference between the lab measurement and the manufacturer's declaration, Intertek measured the rotational speeds of the medium wheel and the small wheel before placing them in the test chambers. It was found that the medium wheel ran at 98 rpm and the small wheel ran at 56 rpm using the original motor and pully supplied by the manufacturer. To realize the same rotational speed, a variable-speed drive

(VSD) was used on the motor of the medium wheel to reduce its speed from 98 rpm to 74 rpm. Because the motor of the small wheel is not VSD-compatible, the original 3.8-cm pully was replaced with a 5.1-cm pully, which increased the wheel speed from 56 rpm to 79 rpm. The difference of rotation speeds (i.e., 79 rpm vs. 74 rpm) is less than the tolerance (±10%) specified in AHRI Standard 1060.

For the second set of wheels, the rotation speed was measured at 21 rpm for the large and small wheels and it was 22 rpm for the medium wheel. In contrast, the manufacturer declared that the rotational speed would be 25 rpm for all three wheels if the motor was run at the rated voltage. Because all motors are VSD-compatible, it is technically possible to achieve the same rpm for all three wheels. However, after considering the resource constraints and the minor difference of rotation speeds being less than the tolerance (±10%) specified in AHRI Standard 1060, Intertek performed the tests without the use of a variable-speed drive for the medium wheel.

Chapter 4: Test Results and Analysis

This chapter presents the test results and their analysis in three aspects of energy exchanger performance: effectiveness, leakage, and pressure drop. Each aspect is discussed with the tested performance results, the change of performance with respect to wheel size, the change of performance with respect to operating conditions. The change of performance with respect to wheel size is evaluated within the context of rating allowances acceptable by AHRI Standard 1060. The change of performance with respect to operating conditions is evaluated against one of the reviewed correlations in Chapter 2.

4.1 Effectiveness Test Results and Analysis

4.1.1 Overview of Effectiveness Test Results

Tables 12 and 13 summarize the effectiveness results for the two sets of wheels respectively. Both the effectiveness and the uncertainties were calculated by Intertek using equations respectively from ASHRAE Standard 84 (ASHRAE 2020a) and ASME Standard PTC 19.1-2013 (ASME 2013). The calculated effectiveness values and uncertainties from Intertek were verified with manual calculations performed as part of this thesis work. In these two tables and hereinafter, the air face velocity for Test 3 is highlighted red to indicate its difference from other tests.

Table 12: Effectiveness and test uncertainty of the first set of wheels

Exchanger	Test No.	Face velocity (m/s)	OA DB/WB temp. (°C)	EA DB/WB temp. (°C)	Effectiveness (%)			Uncertainty (%)		
					ε_s	ε_l	ε_t	ε_s	ε_l	ε_t
W1: small	1	3.048	37.8/26.7	21.1/15.6	68.5	66.2	67.3	0.21	0.82	0.48
	2	3.048	32.2/23.9	21.1/15.6	67.9	66.5	67.1	0.39	1.01	0.66
	3	1.829	37.8/26.7	21.1/15.6	75.0	75.0	75.1	0.70	0.76	0.80
W1: medium	1	3.048	37.8/26.7	21.1/15.6	69.2	67.0	68.1	0.35	0.85	0.57
	2	3.048	32.2/23.9	21.1/15.6	68.7	66.7	67.6	0.42	1.02	0.68
	3	1.829	37.8/26.7	21.1/15.6	75.8	75.1	75.5	0.49	0.74	0.63
W1: large	1	3.048	37.8/26.7	21.1/15.6	68.3	66.3	67.3	0.31	0.82	0.54
	2	3.048	32.2/23.9	21.1/15.6	67.7	66.8	67.2	0.39	1.01	0.66
	3	1.829	37.8/26.7	21.1/15.6	75.5	75.2	75.5	0.47	0.77	0.62
	4	3.048	37.8/28.3	23.9/18.3	68.0	64.3	65.7	0.33	0.92	0.64
	5	3.048	37.8/23.3	21.1/15.6	69.2	69.0	69.2	0.31	1.34	0.62
	6	3.048	26.7/20.0	20.0/14.4	66.8	67.7	67.4	0.56	1.34	0.87
	7	3.048	23.9/21.1	18.3/14.4	64.3	65.5	65.2	0.66	1.00	0.77

Table 13: Effectiveness and test uncertainty of the second set of wheels

Exchanger	Test No.	Face velocity (m/s)	OA DB/WB temp. (°C)	EA DB/WB temp. (°C)	Effectiveness (%)			Uncertainty (%)		
					ε_s	ε_l	ε_t	ε_s	ε_l	ε_t
W2: small	1	3.302	37.8/26.7	21.1/15.6	71.8	64.3	67.6	0.39	0.84	0.58
	2	3.302	32.2/23.9	21.1/15.6	71.7	66.5	68.6	0.47	0.97	0.69
	3	2.311	37.8/26.7	21.1/15.6	76.3	73.5	74.8	0.74	0.78	0.83
W2: medium	1	3.302	37.8/26.7	21.1/15.6	72.1	63.3	67.2	0.35	0.85	0.56
	2	3.302	32.2/23.9	21.1/15.6	72.0	66.0	68.5	0.42	1.00	0.67
	3	2.311	37.8/26.7	21.1/15.6	77.1	72.9	74.8	0.64	0.76	0.74
W2: large	1	3.302	37.8/26.7	21.1/15.6	73.0	64.4	68.1	0.36	0.82	0.55
	2	3.302	32.2/23.9	21.1/15.6	71.8	67.4	69.3	0.42	1.03	0.67
	3	2.311	37.8/26.7	21.1/15.6	76.8	72.7	74.5	0.45	0.86	0.60
	4	3.302	37.8/28.3	23.9/18.3	73.2	63.0	66.7	0.38	0.94	0.64
	5	3.302	37.8/23.3	21.1/15.6	73.0	67.9	71.0	0.35	1.32	0.62
	6	3.302	26.7/20.0	20.0/14.4	71.5	70.7	71.1	0.60	1.40	0.91
	7	3.302	23.9/21.1	18.3/14.4	70.1	72.3	71.8	0.69	0.98	0.77

It can be observed from the above two tables that for a given test the total effectiveness mainly lies in between the sensible effectiveness and the latent effectiveness (Simonson and Besant 1998). In addition, the sensible effectiveness is higher than the latent effectiveness for most of the tests. However, when the two airstreams have low temperature difference but high difference of water vapor pressure (i.e., Test 6 and Test 7), the latent effectiveness may be higher.

The uncertainties of the effectiveness test results satisfy ASHRAE Standard 84, which requires the following:

$$U(\varepsilon_s) < 5\% \quad (22)$$

$$U(\varepsilon_l) < 7\% \quad (23)$$

$$U(\varepsilon_t) < \frac{|\varepsilon_l - \varepsilon_t|5\% + |\varepsilon_s - \varepsilon_t|7\%}{|\varepsilon_l - \varepsilon_s|} \quad (24)$$

4.1.2 The Change of Effectiveness with Wheel Sizes

The sensible effectiveness, latent effectiveness, and total effectiveness are plotted against the airflow rate to investigate whether they change with wheel sizes belonging to the same TSG. Figures 6-8 are for the first set of wheels, data are shown in and Figures 9-11 are for the second set of wheels. In these figures, the test results are shown as data labels while uncertainties are indicated as error bars. If the error bars of any two wheels with different sizes overlap with each other, it can be reasonably concluded that the two wheels have the same effectiveness values after accounting for the test uncertainties.

The following can be observed for the first set of wheels (Figures 6-8):

- Most of the sensible effectiveness values exhibited consistency throughout different wheel sizes under the same test conditions. The exceptions include 1) under the Test 1 condition, the medium wheel and the other two wheels did not have any overlap between their possible ranges; and 2) under the Test 2 condition, the large wheel and the medium wheel did not show any overlap in their possible ranges of sensible effectiveness. However, the gap between the error bars is minimal.

- Under the same test conditions, all latent effectiveness values showed consistency across different wheel sizes.
- Under the same test conditions, all total effectiveness values showed consistency across different wheel sizes.

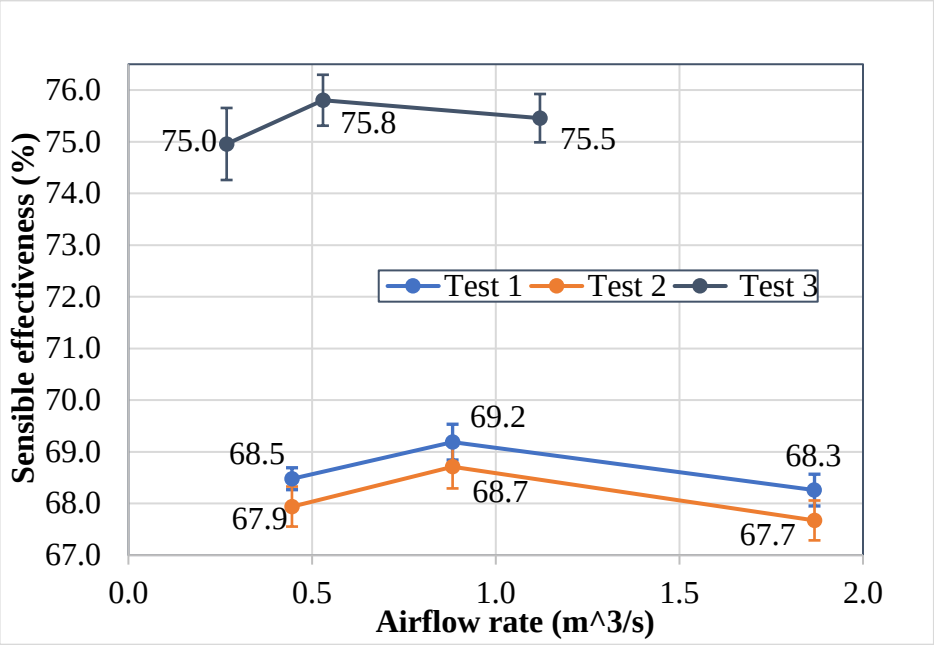

Figure 6: The change of sensible effectiveness with wheel size for the first set of wheels

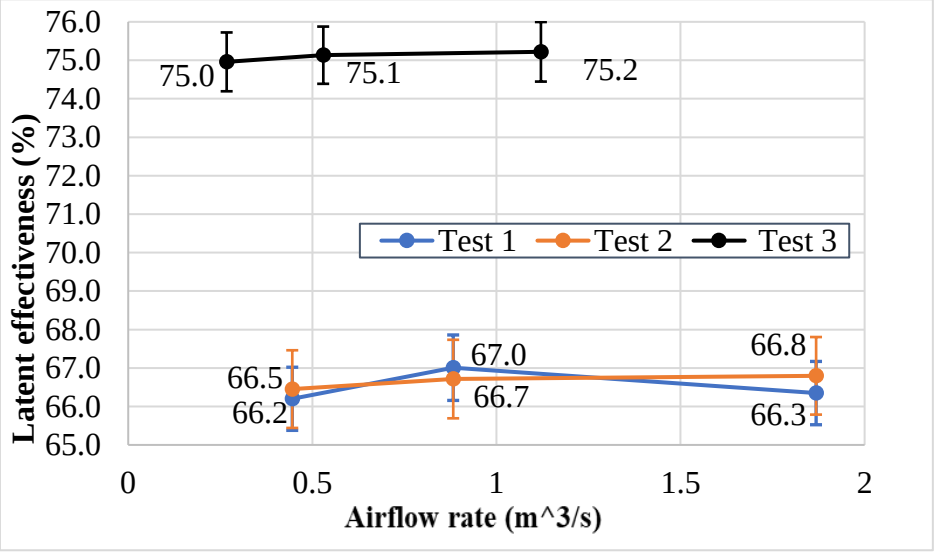

Figure 7: The change of latent effectiveness with wheel size for the first set of wheels

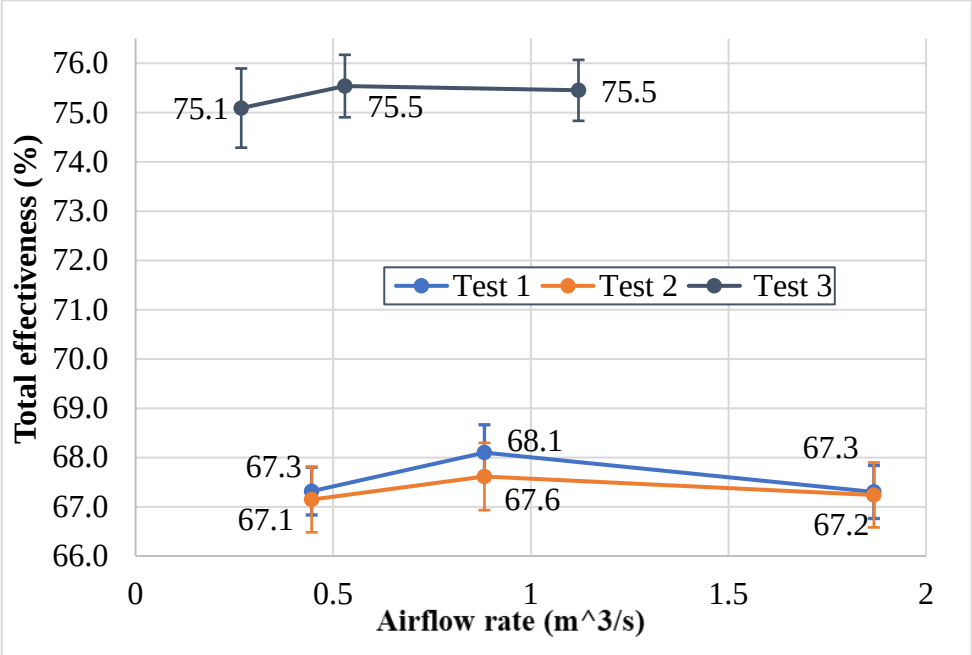

Figure 8: The change of total effectiveness with wheel size for the first set of wheels

The following can be observed for the second set of wheels (Figures 9-11) :

- Except for the large and medium wheels under the Test 1 condition, all other pairwise comparisons demonstrated the consistency of sensible effectiveness values.
- Under the same test conditions, all latent effectiveness values showed consistency across different wheel sizes.
- Under the same test conditions, all total effectiveness values showed consistency across different wheel sizes.

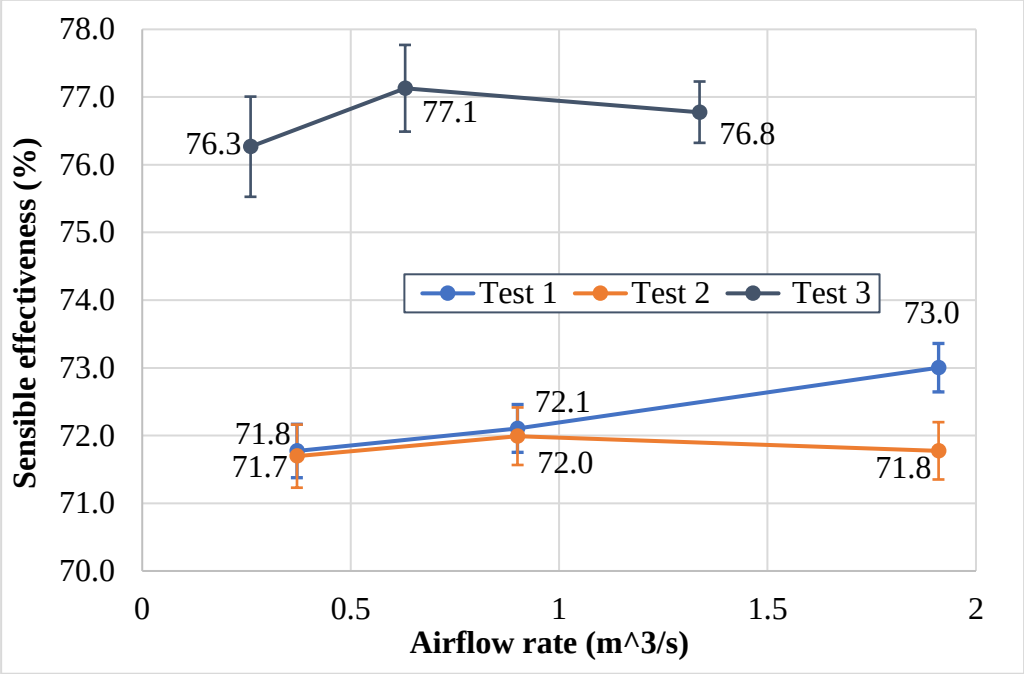

Figure 9: The change of sensible effectiveness with wheel size for the second set of wheels

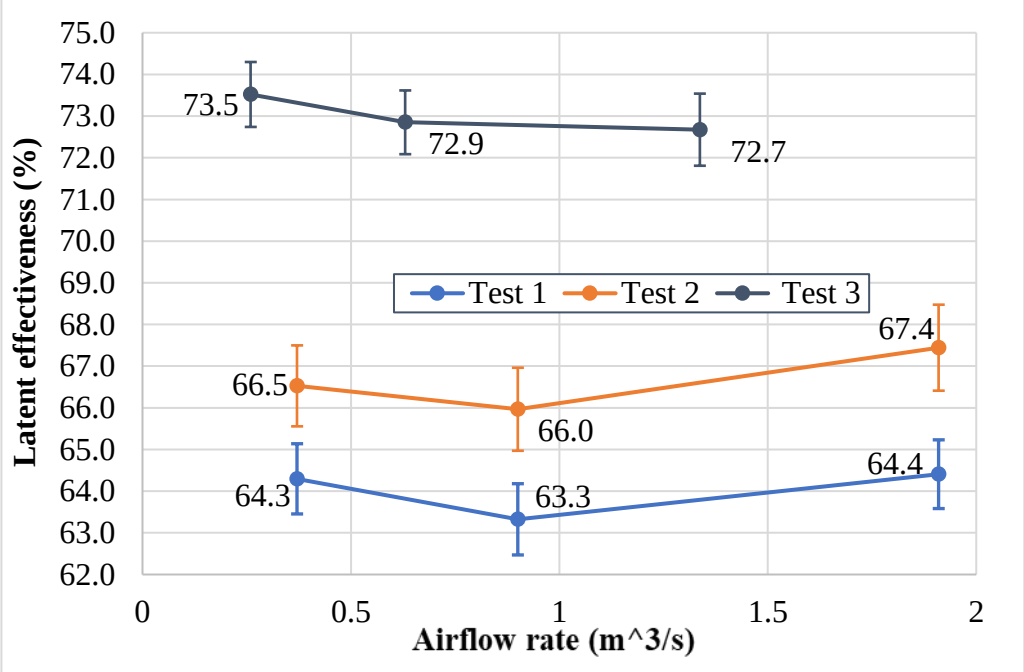

Figure 10: The change of latent effectiveness with wheel size for the second set of wheels

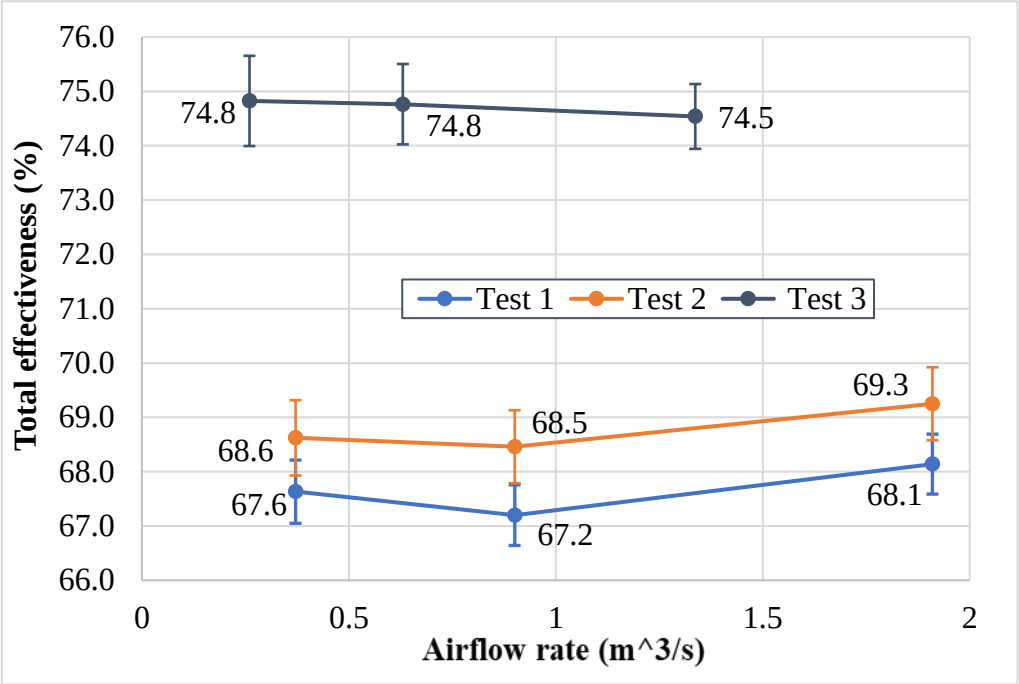

Figure 11: The change of total effectiveness with wheel size for the second set of wheels

A major goal of this research is to validate the extrapolation approach that AHRI employs to rate air-to-air energy recovery ventilators equipment with an airflow rate of more than 2.36 m^3/s. This extrapolation approach allows large energy exchangers to be rated the same as smaller energy exchangers if they belong to the same TSG (the term "Basic Model Group" is used in AHRI). Therefore, it is crucial to investigate how the effectiveness ratings can overlap after accounting for the acceptable allowance by AHRI Standard 1060.

AHRI Standard 1060 (AHRI 2018) states the following allowances for sensible effectiveness and latent effectiveness:

- "Test results for Sensible Effectiveness shall not be lower than the Published Rating by more than: (1) the sum of four relative percentage points and one absolute percentage point, or (2) two absolute percentage points below the Published Rating, whichever is greater."

- "Test results for Latent Effectiveness shall not be lower than the Published Rating by more than (1) the sum of six relative percentage points and one absolute percentage point, or (2) two absolute percentage points below the Published Rating, whichever is greater."

Thus, based on the test results of each wheel, the ranges of published ratings that satisfy the allowance requirement of ASHRI Standard 1060 can be calculated. Figures 12 and 13 show the ranges of possible published ratings for the first set that satisfy the allowance requirements of AHRI Standard 1060 while Figures 14 and 15 are for the second set. In these figures, the ranges of published ratings are presented as error bars. In addition, only upward bars are shown because manufacturers will unlikely underrate the performance of their products. Figures 12-15 show that the allowances satisfying AHRI Standard 1060 are much wider than the test uncertainties due to measurement inaccuracy. Because of the wide allowances, the acceptable rating ranges under the same test condition have much overlap with each other between different wheel sizes. This observation provides strong support of AHRI's extrapolation approach for effectiveness rating.

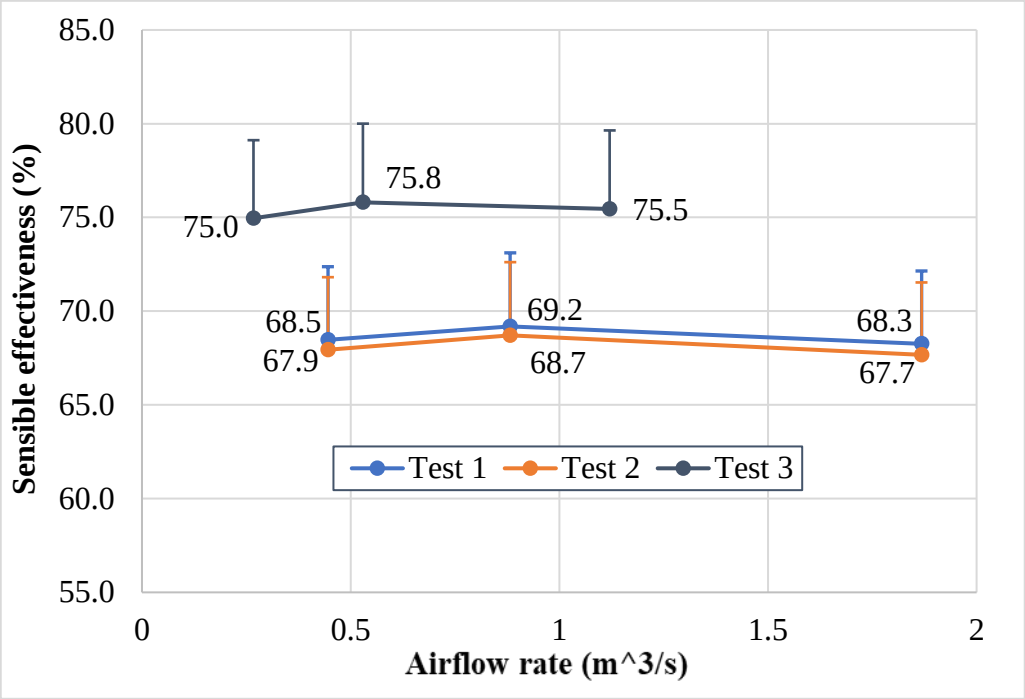

Figure 12: Acceptable rating ranges of sensible effectiveness for the first set of wheels

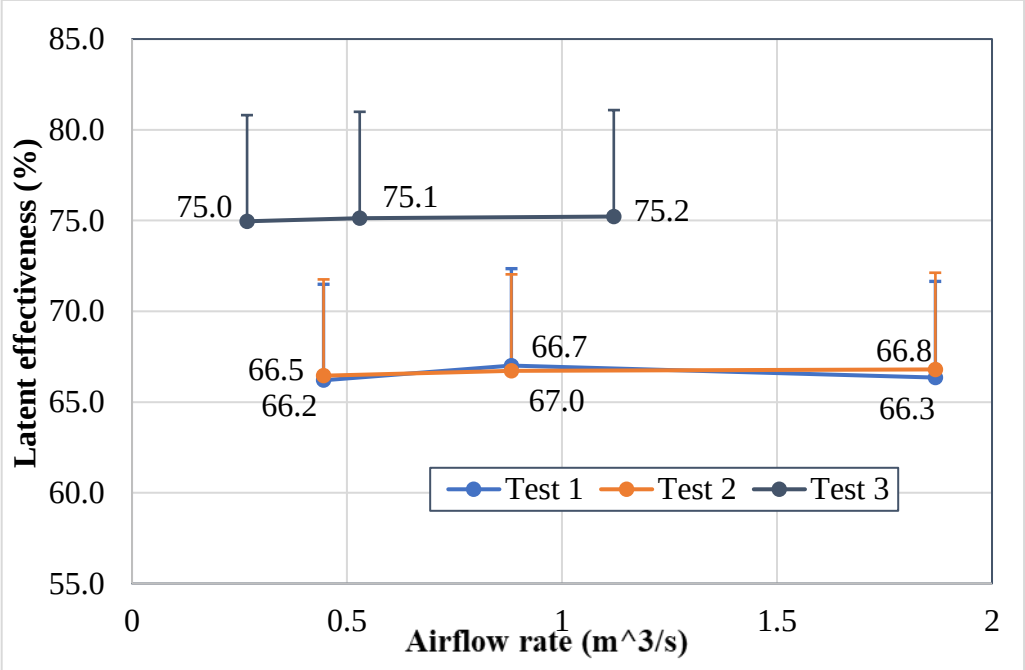

Figure 13: Acceptable rating ranges of latent effectiveness for the first set of wheels

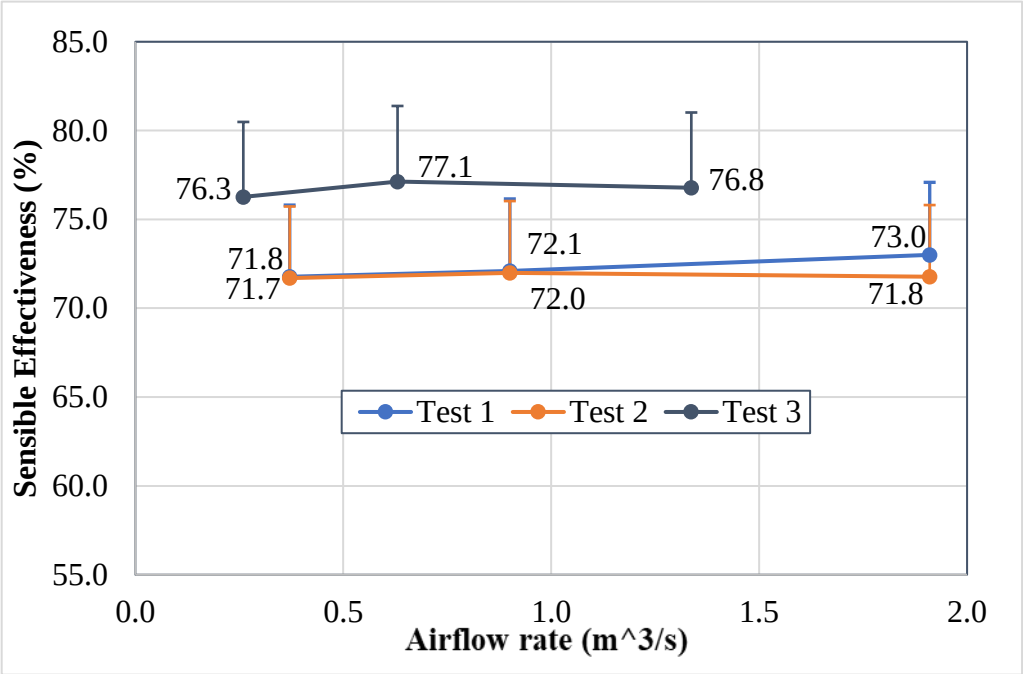

Figure 14: Acceptable rating ranges of sensible effectiveness for the second set of wheels

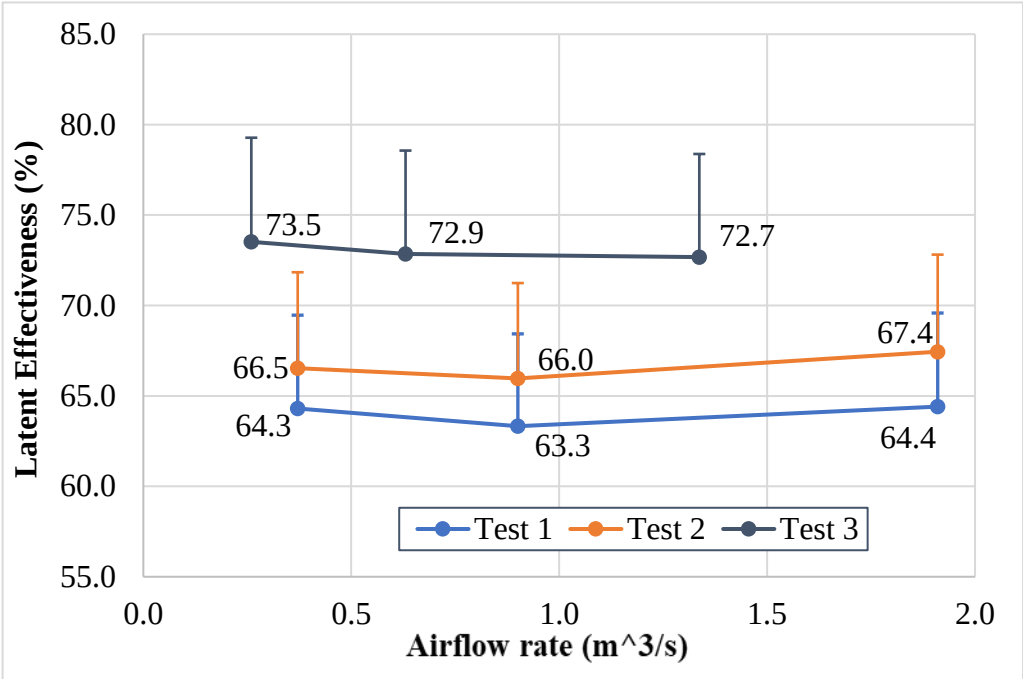

Figure 15: Acceptable rating ranges of latent effectiveness for the second set of wheels

4.1.3 The Change of Effectiveness with the Psychrometric Conditions of Supply and Exhaust Air

For both two sets of wheels, the large wheel has the most different test conditions, so it is used to study the change of effectiveness with the psychrometric conditions of inlet air. To facilitate the comparison, the operating condition factor (H*) presented by Simonson and Besant (1999) is used as a unifying measure to indicate the inlet air conditions. The dimensionless factor H* refers to the ratio of latent to sensible energy differences between the supply air and exhaust air, and it is calculated as follows:

$$H^* = 2500\frac{\Delta W}{\Delta T} = \frac{\Delta H_l}{\Delta H_s} = \left(\frac{\Delta H_s}{\Delta H_t}\right)^{-1} - 1 \qquad (25)$$

where, ΔW, ΔT, ΔH_s, ΔH_l, ΔH_t respectively represents the humidity ratio difference (kg/kg), the dry-bulb temperature difference (°C), the sensible energy difference, the latent energy difference, and the total energy difference between the supply air and the exhaust air.

A single value of H* can represent numerous inlet air conditions with supply air and exhaust air having different air properties. Figure 16 is from Simonson and Besant (1999) and it shows multiple values of H* that were obtained by changing supply air conditions while keeping exhaust air at 24°C and 50% relative humidity. In this figure, all points on any straight line have the same value of H* even though the supply air conditions are different.

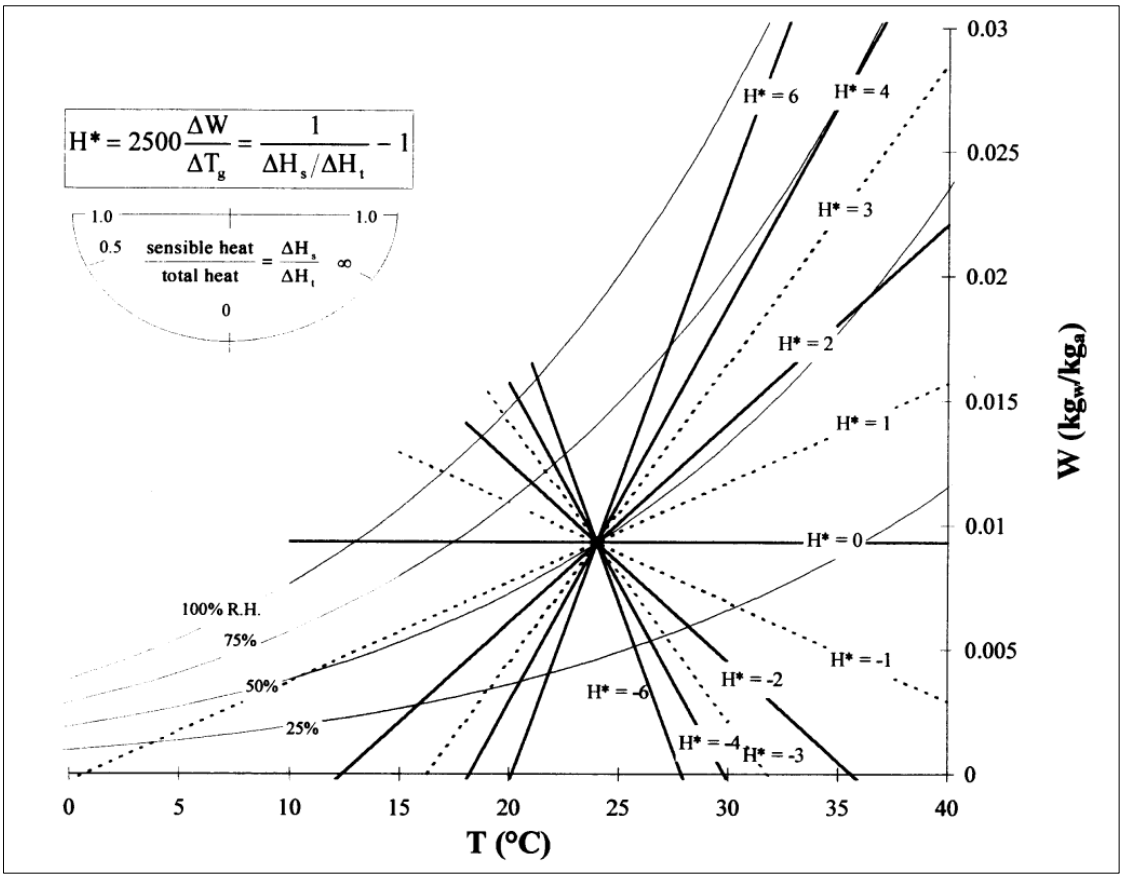

Figure 16: The operating factor (H*) for different supply air conditions with exhaust air conditions fixed at 2°C (75°F) and 50% relative humidity (Simonson and Besant 1999)

The values of H* for the tests of the two large wheels were calculated and plotted as shown in Figures 17-22. Because Test 3 has a different air face velocity from the other tests, it is not included.

Both Figures 17 and 20 show the relationship between the sensible effectiveness and H*. It is observed that the sensible effectiveness decreases as H* increases, which agrees with the finding from Simonson and Besant (1999). In their work, Simonson and Besant indicated that the sensible effectiveness and H* had a strict linear relationship. Based on our test results, the value of R^2 in the linear regression is 0.86 and 0.56 for the first and the second wheel respectively (Figures 17 and 20).

Figures 18 and 21 show the relationship between the latent effectiveness and H*, which does not show any strong and consistent relationship between the two variables. This observation is different from the previous work (Simonson and Besant 1999), which indicated that for positive H* values, the latent effectiveness increased with H* but it became saturated until H* =2. Because the linear correlation between latent effectiveness and H* does not exist for the entire range of H*, the trendlines are not shown in these two figures.

Figures 19 and 22 show the relationship between the total effectiveness and H*, which has a decreasing linear relationship for the first large wheel but almost no clear relationship for the second wheel. This observation is different from the previous work (Simonson and Besant 1999), which indicated that for positive H* values, the total effectiveness increases with H* at the beginning but it almost saturates until H*=3. Because the linear correlation between total effectiveness and H* does not exist for the entire range of H*, the trendlines are not shown in these two figures.

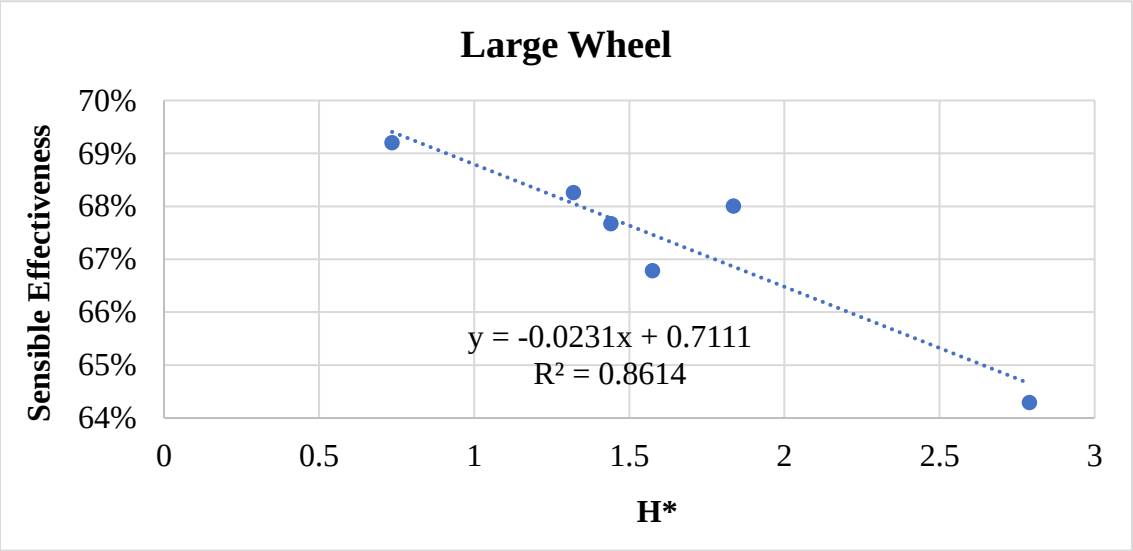

Figure 17: The change of sensible effectiveness with H* for the first set of wheels

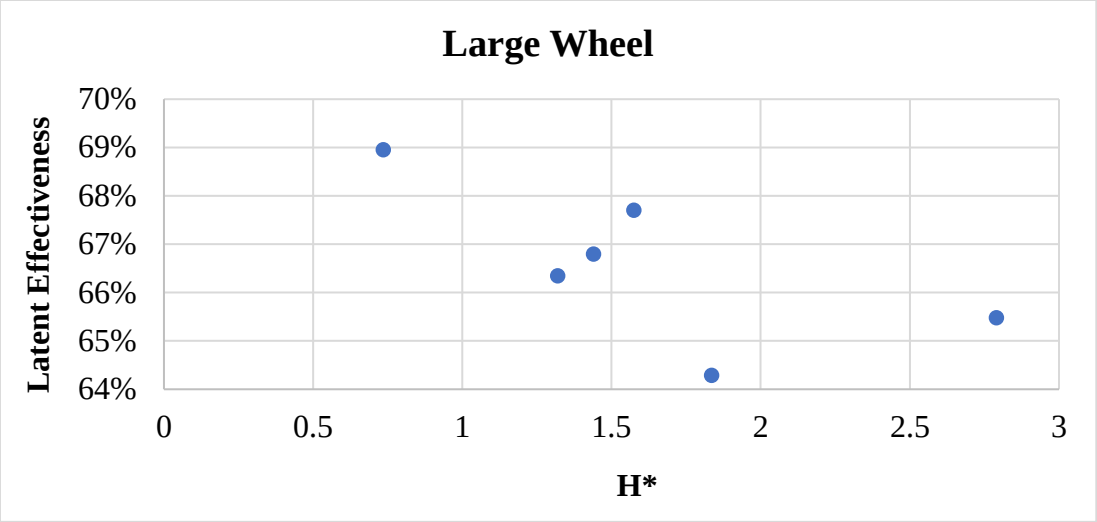

Figure 18: The change of latent effectiveness with H* for the first set of wheels

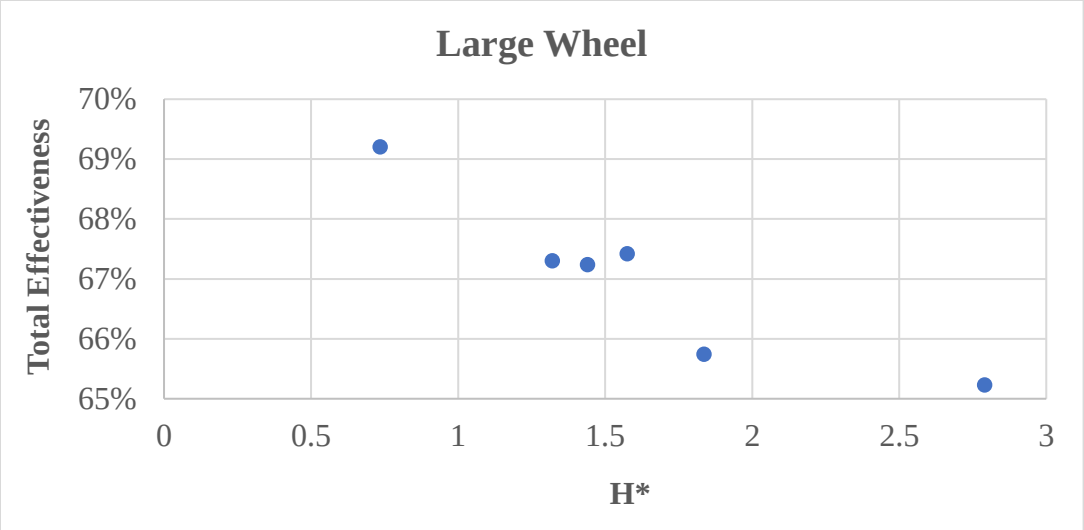

Figure 19: The change of total effectiveness with H* for the first set of wheels

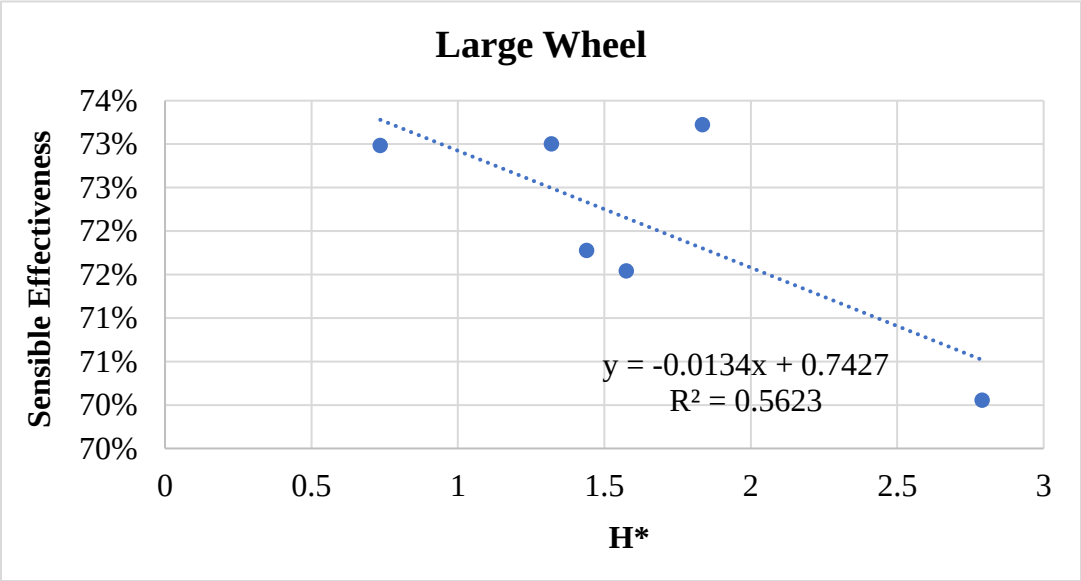

Figure 20: The change of sensible effectiveness with H* for the second set of wheels

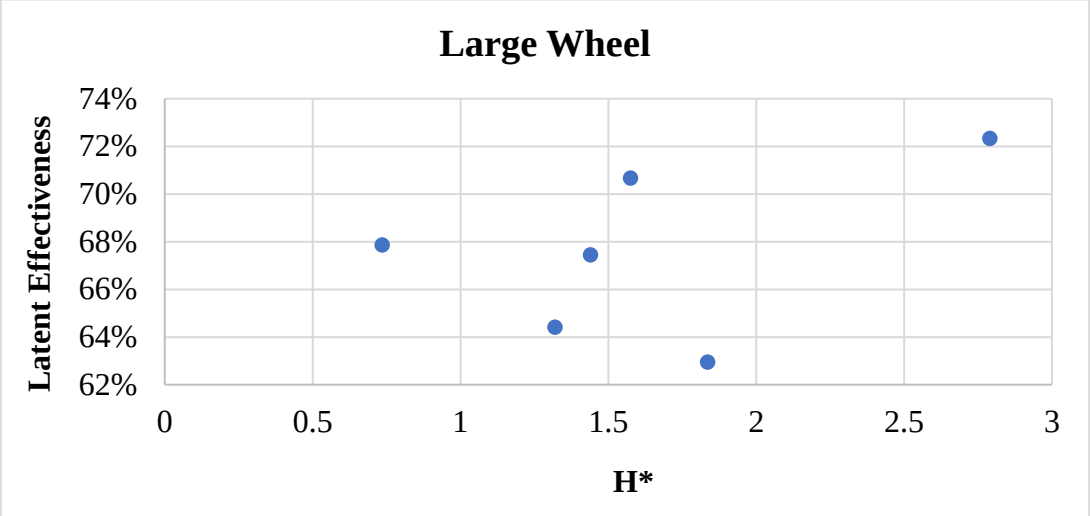

Figure 21: The change of latent effectiveness with H* for the second set of wheels

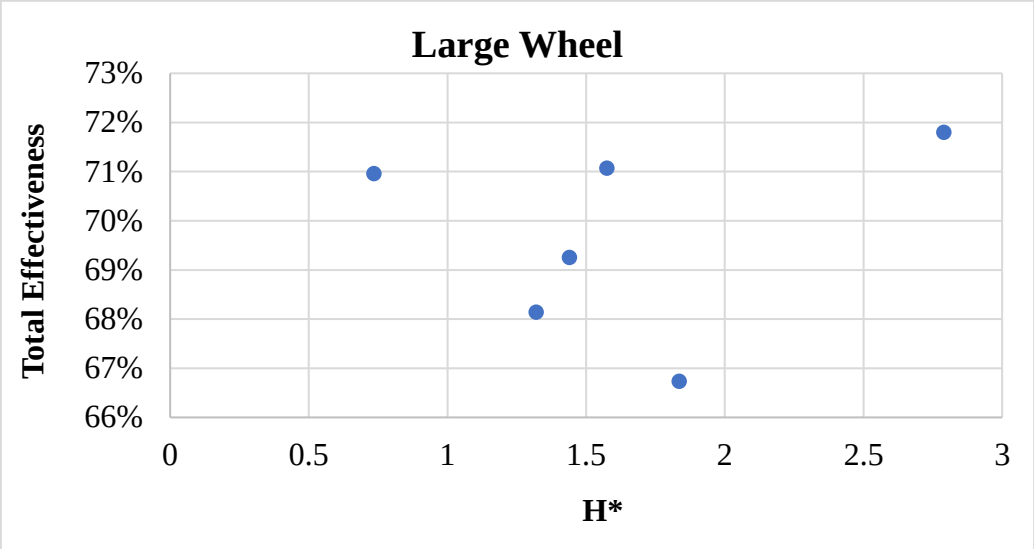

Figure 22: The change of total effectiveness with H* for the second set of wheels

4.1.4 The Change of Effectiveness with Air Face Velocity

The change of effectiveness with air face velocity can be observed by comparing the effectiveness between Test 1 and Test 3. These two tests differ only with respect to the air face velocity. Figures 23 and 24 show the results for the two sets of wheels respectively. In these two figures, the vertical axis represents the ratio of effectiveness between Test 3 and Test 1.

For the first set of wheels (Figure 23), the effectiveness increased by approximately 10% (sensible), 13% (latent) and 12% (total) due to the reduction of air face velocity by 40% from Test 1 to Test 3.

For the second set of wheels (Figure 24), the effectiveness increased by approximately 6% (sensible), 14% (latent) and 11% (total) due to the reduction of air face velocity by 30% from Test 1 to Test 3.

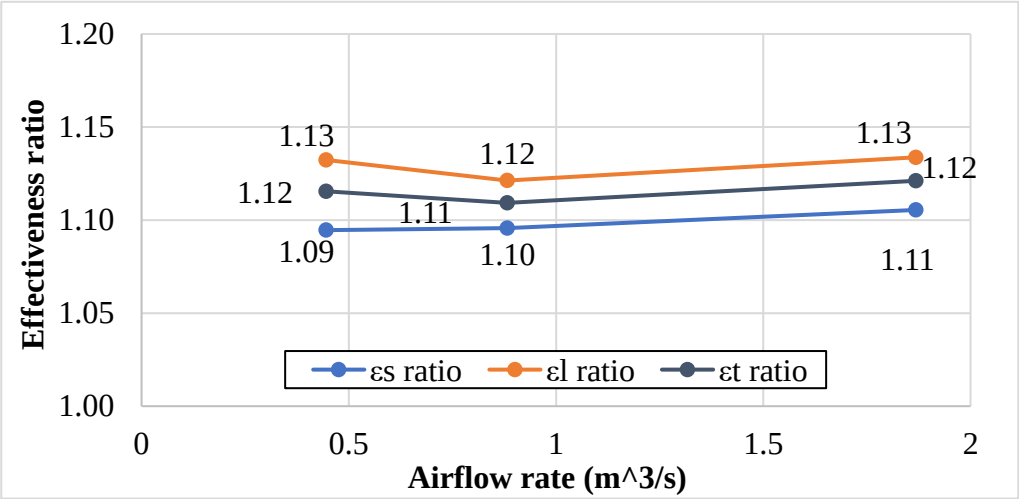

Figure 23: The ratio of effectiveness between Test 3 and Test 1 as the air face velocity is reduced by 40% for the first set of wheels

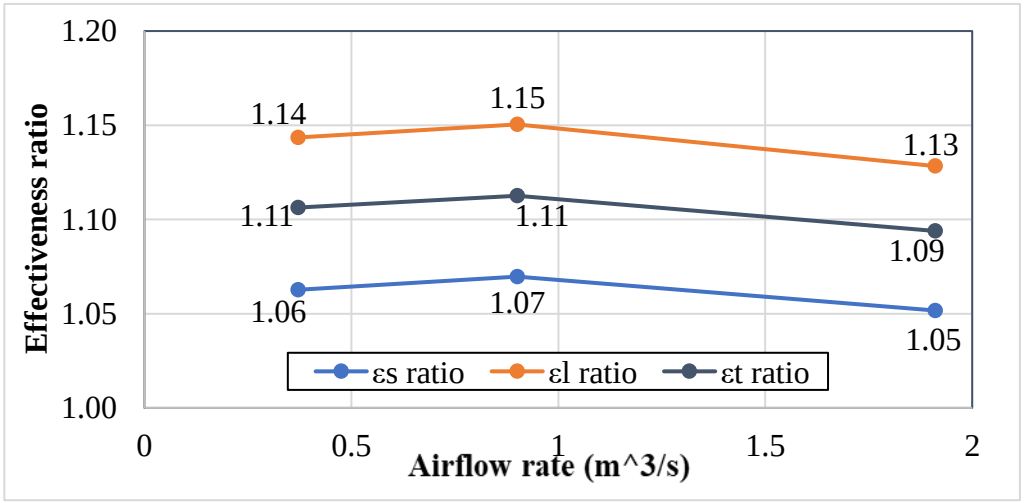

Figure 24: The ratio of effectiveness between Test 3 and Test 1 as the air face velocity is reduced by 30% for the second set of wheels

4.2 Trace Gas Tests

4.2.1 Tracer Gas Test Results

Tables 14 and 15 summarize the tracer gas test results for the two sets of wheels respectively. The EATR, OACF and the uncertainties were from Intertek's test reports and they were calculated according to ASHRAE Standard 84 (ASHRAE 2020a) and ASME Standard PTC 19.1-2013 (ASME 2013), respectively. All wheels has two tracer gas tests with pressure

differential of 0 an -500 Pa. The test results presented in these two tables are used to create the plots in the following subsections.

Table 14: EATR, OACF, and their uncertainties of the first set of wheels

Exchanger	Test No.	Airflow rate (m^3/s)	Pressure differential, P_2-P_3 (Pa)	EATR (%)	EATR uncertainty (%)	OACF	OACF uncertainty
W1: small	4	0.445	0	3.11	0.075	1.11	0.003
	5	0.445	-500	17.99	0.067	0.84	0.003
W1: medium	4	0.883	0	3.85	0.125	1.12	0.004
	5	0.883	-500	21.44	0.054	0.80	0.004
W1: large	8	1.867	0	3.91	0.098	1.05	0.004
	9	1.867	-500	10.75	0.088	0.91	0.004

Table 15: EATR, OACF, and their uncertainties of the second set of wheels

Exchanger	Test No.	Airflow rate (m^3/s)	Pressure differential, P_2-P_3 (Pa)	EATR (%)	EATR uncertainty (%)	OACF	OACF uncertainty
W2: small	4	0.371	0	2.97	0.082	1.14	0.005
	5	0.371	-500	19.53	0.078	0.82	0.005
W2: medium	4	0.900	0	3.13	0.069	1.09	0.004
	5	0.900	-500	11.85	0.064	0.91	0.004
W2: large	8	1.909	0	3.25	0.066	1.03	0.004
	9	1.909	-500	10.49	0.060	0.92	0.004

The uncertainties of tracer gas test results satisfy ASHRAE Standard 84, which requires:

$$U(EATR) < 3\% \quad (26)$$

$$U(OACF) < 0.02 \quad (27)$$

4.2.2 The Change of EATR with Wheel Sizes

The EATR is plotted against the airflow rate to investigate whether the EATR changes with different wheel sizes of the same TSG. Figure 25 and Figure 26 are respectively for the two

sets of wheels. Error bars are plotted to indicate the uncertainties, however, they are invisible because of their small values relative to the EATR.

When the pressure differential is zero, the EATR changes slightly with the wheel size for both sets of wheels. To clearly view if the uncertainty bars overlap, the data set with zero pressure differential are plotted only and it can be seen in Figures 27 and 28. These two figures indicate that except for the large and medium wheels of the first set, the EATR generally does not exhibit consistency across different wheel sizes after accounting for test uncertainties.

When the pressure differential is -500 Pa, the EATR values are much higher than those at zero pressure differential. All tested EATRs do not exhibit consistency across different wheel sizes, even after considering the test uncertainties. It has been observed that the two set of wheels have different patterns of how EATR changes with wheel sizes. For the first set, the medium wheel has the highest EATR while for the second set, the small wheel has the highest EATR.

EATR is a performance metric that measures the leakage across the two airstreams, this leakage can attribute to carryover and seal leakage. Per ASHRAE (2020b), the carryover can be calculated as:

$$Carryover = \frac{L*\varphi*rpm}{0.5*V} * 100\% \quad (28)$$

where, L is the wheel depth (m), φ is the porosity indicating the void volume of the matrix, rpm is the wheel rotational speed per minute, V is the air face velocity (m/s).

The equation above shows that for different wheels of the same TSG, theoretically, the percentage of carryover does not change with size.

Regarding the crossflow leakage caused by seals, the seals placed in the middle beam and spokes are relevant. The length of seals is proportional to the wheel diameter, while the airflow rate is proportional to the square of wheel diameter. Therefore, if the number of beams and spokes are the same for different wheel sizes of the same TSG, the percentage of seal leakage is inversely proportional to the wheel diameter. In other words, the percentage of seal leakage is smaller for larger wheels. The above trend is observed for the second set of wheels (Figure 26) at the pressure differential of -500 Pa but not for the first set of wheels (Figure 25).

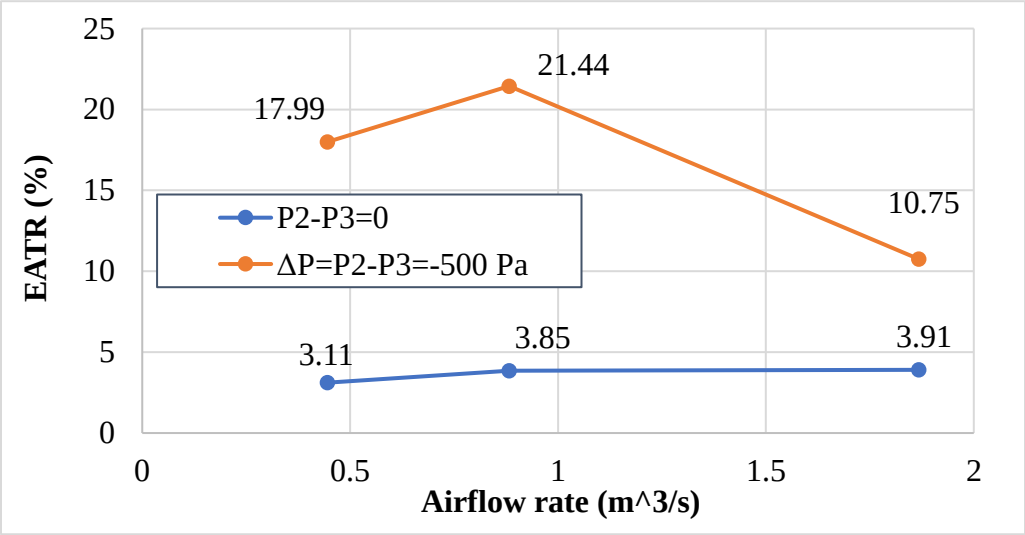

Figure 25: The change of EATR with wheel size for the first set of wheels

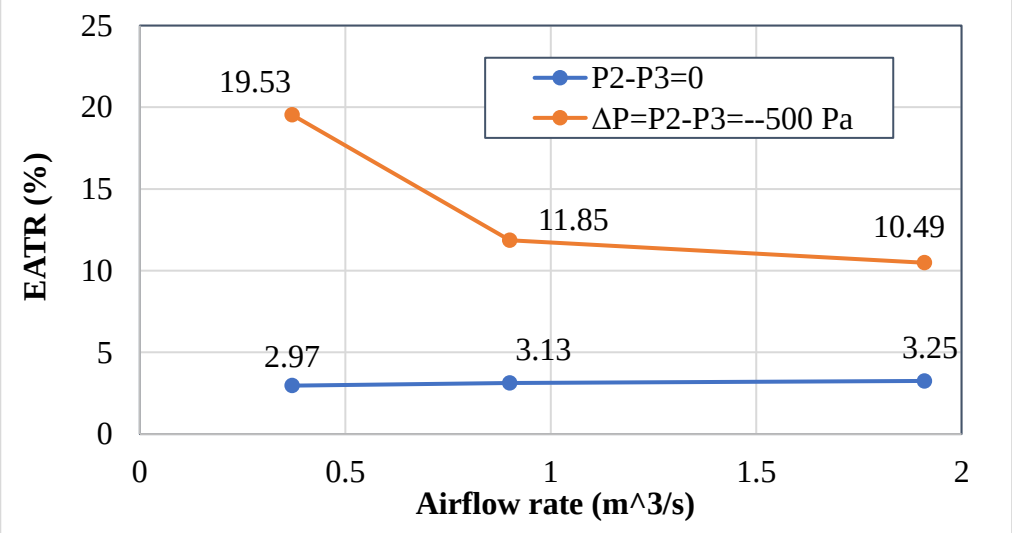

Figure 26: The change of EATR with wheel size for the second set of wheels

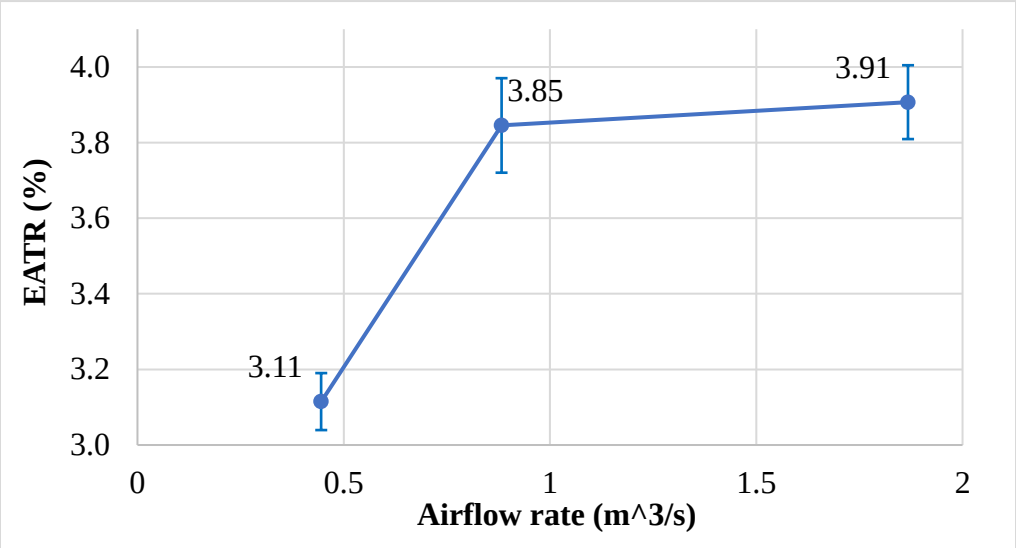

Figure 27: The change of EATR with wheel size at zero pressure differential for the first set of wheels

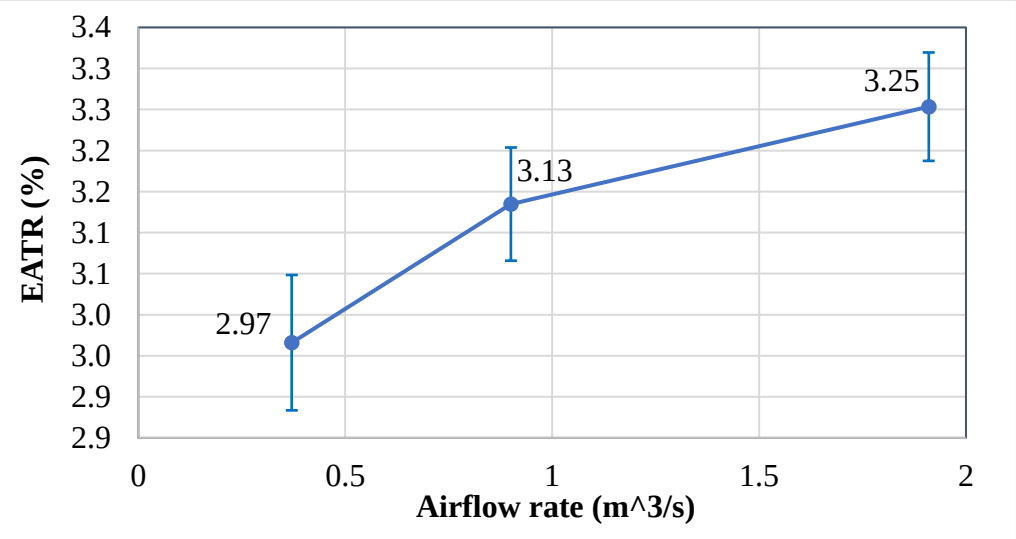

Figure 28: The change of EATR with wheel size at zero pressure differential for the second set of wheels

Similar to what has been performed for the effectiveness results, it is important to understand the change of EATR with wheel size in the context of rating allowances. AHRI Standard 1060 specifies that "Test results for EATR shall not be more than one absolute percentage point greater than the Published Rating". Thus, 1% is marked as the magnitude of error bars for all test points. Figures 29 and 30 show the plots for the two sets of wheels. Only

the downward bars are shown because manufacturers will unlikely overestimate the EATR values.

By comparing Figures 25 and 26 to Figures 29 and 30, we can find that the allowances satisfying AHRI Standard 1060 are much wider than the test uncertainties because of measurement inaccuracy. The allowable rating manufacturers' ranges under the test condition of zero pressure differential overlaps with each other between different wheel sizes. However, this is not the case for most tests with pressure differential of -500 Pa. If the observations based on the test results of two sets of wheels can be generalized, it can be concluded that for EATR rating, the current extrapolation approach in AHRI Standard 1060 is valid when the pressure differential is zero. However, this approach could overestimate the EATR of large wheels with airflow rate more than 2.36 m^3/s if the pressure differential is -500 Pa or lower. This does not impose a problem from the consumer perspective because the overestimation of EATR conservatively evaluates the leakage performance of wheels.

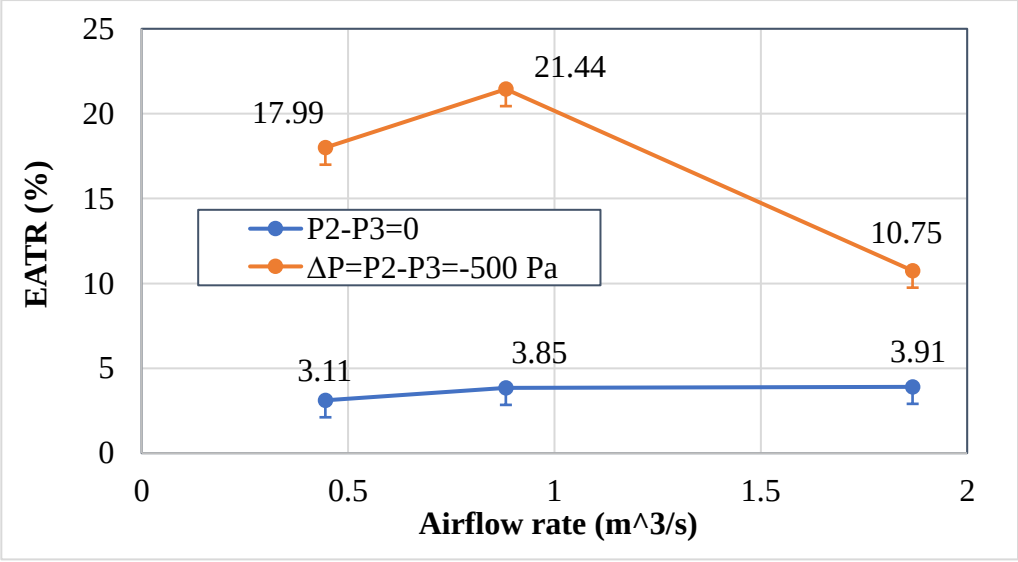

Figure 29: Acceptable rating ranges of EATR for the first set of wheels

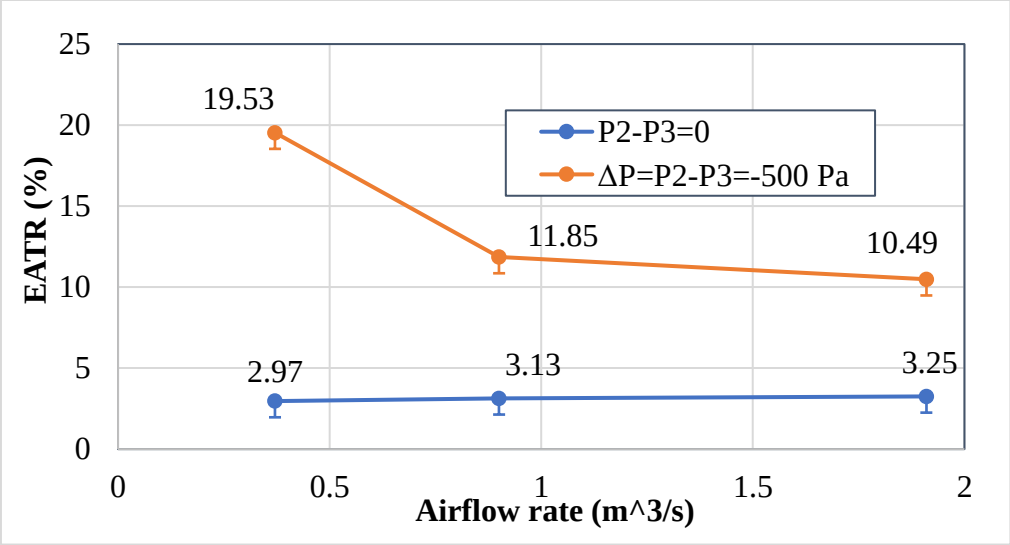

Figure 30: Acceptable rating ranges of EATR for the second set of wheels

4.2.3 The Change of OACF with Wheel Sizes

The change of OACF with wheel sizes is investigated similarly to EATR. The OACF is plotted against the airflow rate for the two sets of wheels as seen in Figures 31 and 32. Error bars are employed to show the uncertainties, but they are not visible because of their small values relative to the OACF. These two figures lead to the following observations:

- At zero pressure differential, the OACF is between 1.05 and 1.12 for the firsts set of wheels, and between 1.03 and 1.14 for the second set of wheels. At zero differential pressure, the crossflow leakage is expected to be minimal. External leakage is the main reason of mass air difference between Station 1(m_1) and Station 2 (m_2). Because the out seals are approximately proportional to the wheel diameter while the airflow rate is proportional to the square of the wheel diameter, it is reasonable to expect that the OACF decreases with the wheel size. This trend is observed for the second set of wheels. However, for the first set of wheels, the highest OACF occurs at the medium wheel.

- At the pressure differential of -500 Pa, the OACF has a value of less than 1. This is because the transfer of air from the exhaust to supply is higher than the external leakage.
- For both sets of wheels, OACF does not show strict consistency across different wheel sizes, even after considering the test uncertainties.

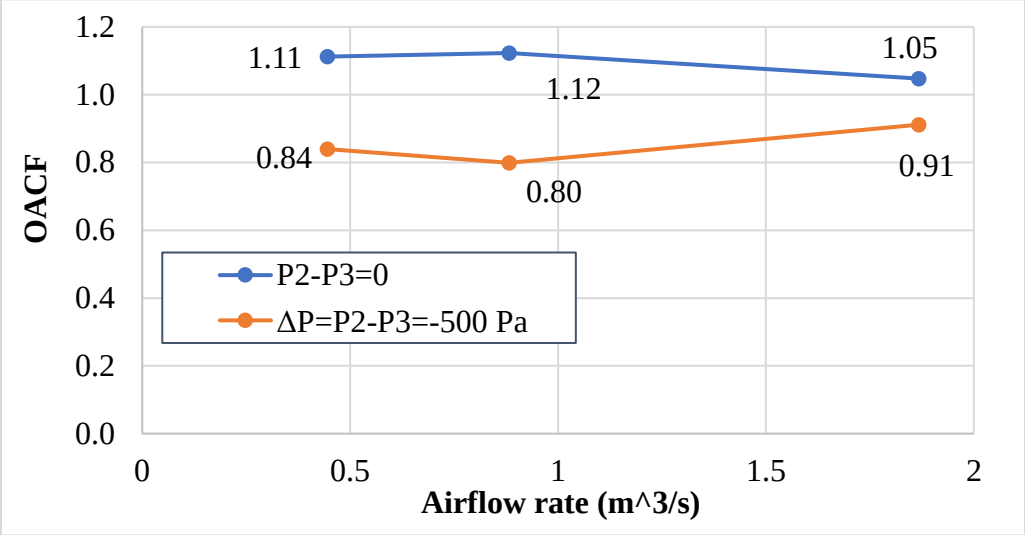

Figure 31: The change of OACF with wheel size for the first set of wheels

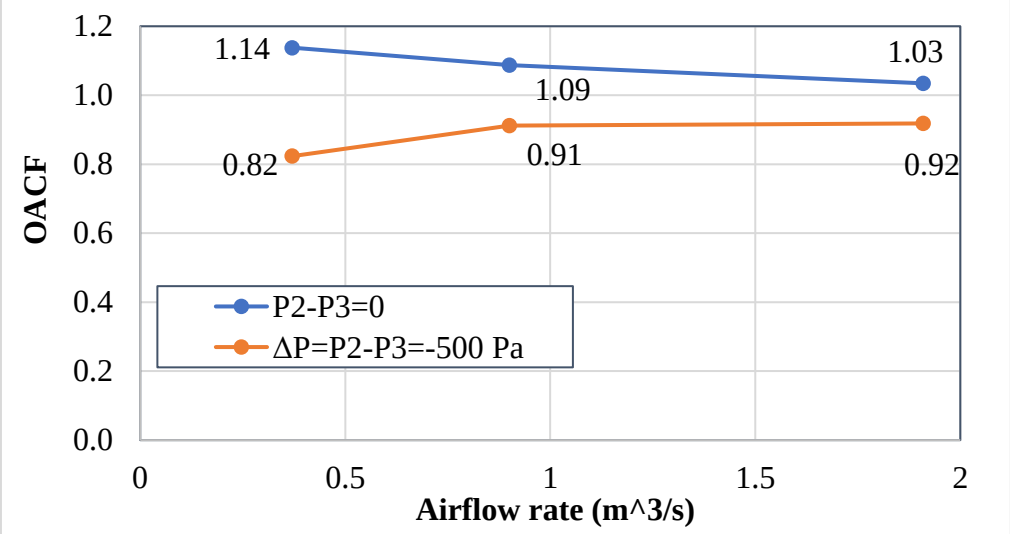

Figure 32: The change of OACF with wheel size for the second set of wheels

AHRI Standard 1060 specifies the allowance for OACF as follows:

- "If the OACF Published Rating is less than 0.91, then the test results shall be less than or equal to 1.00 and greater than or equal to 90% of the Published Rating."
- "If the OACF Published Rating is greater than or equal to 0.91 and less than or equal to 1.11, then the test results shall be greater than or equal to 90% of the Published Rating and less than or equal to 110% of the Published Rating."
- "If the OACF Published Rating is greater than 1.11, then the test results shall be greater than or equal to 1.00 and less than or equal to 110% of the Published Rating."

To calculate the allowance for OACF rating, it is assumed that the published rating of OACF takes the average value for the whole set of wheels at each tracer gas test condition. Then, the minimum and maximum OACF can be calculated and they are the ranges of test results that lead to the same published rating of OACF Figures 33 and 34 are for the two sets of wheels. These two figures show that the ranges of test results satisfying AHRI Standard 1060 are much wider than the test uncertainties due to measurement inaccuracy. Under the same test condition, the ranges of acceptable test results have much overlap with each other between different wheel sizes. This observation provides strong support of AHRI's extrapolation approach for OACF rating.

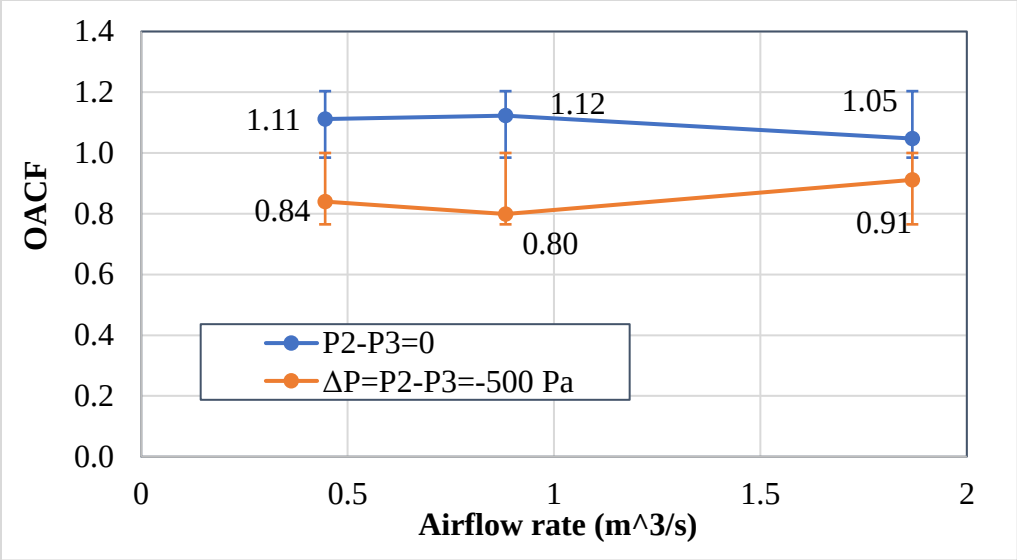

Figure 33: Acceptable rating ranges of OACF for the first set of wheels

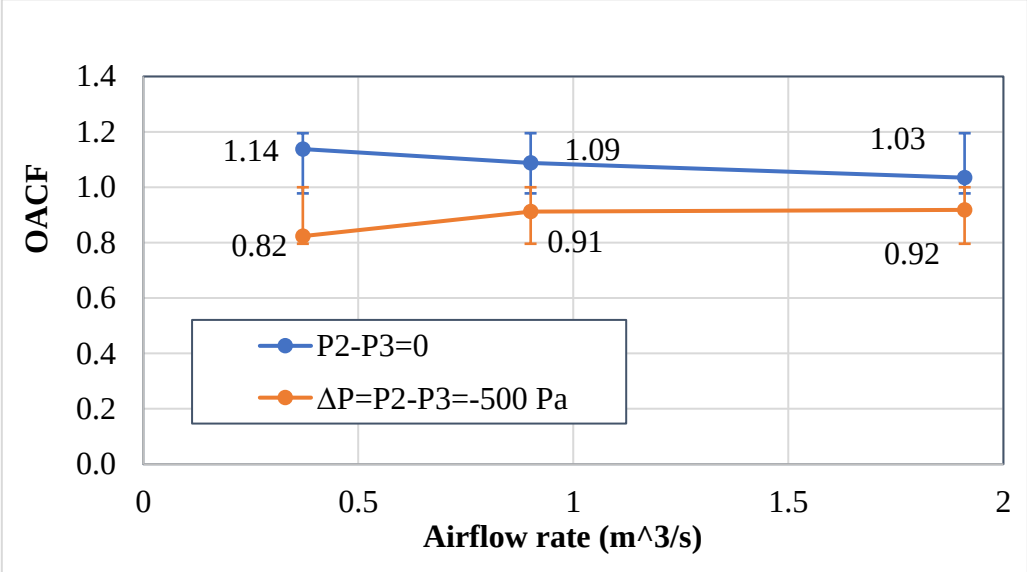

Figure 34: Acceptable rating ranges of OACF for the second set of wheels

4.3 Pressure Drop Tests

4.3.1 Pressure Drop Results

There were no tests dedicated to pressure drops. Instead, pressure drops in both supply and exhaust airstreams were measured in all effectiveness and tracer gas tests. Tables 16 and 17 list the results. The airflow rate for Test 3 is highlighted red because it is different from other tests.

Table 16: Pressure drops of the first set of wheels

Exchanger	Test No.	Test type	Airflow rate (m^3/s)	Pressure drop (Pa)	
				Supply airstream	Exhaust airstream
W1: small	1	Eff.	0.445	202	199
	2	Eff.	0.445	197	197
	3	Eff.	0.267	112	110
	4	Tracer	0.445	199	197
	5	Tracer	0.445	164	172
W1: medium	1	Eff.	0.882	167	167
	2	Eff.	0.882	164	164
	3	Eff.	0.529	97	95
	4	Tracer	0.882	159	162
	5	Tracer	0.882	139	144
W1: large	1	Eff.	1.867	149	157
	2	Eff.	1.867	149	147
	3	Eff.	1.121	85	87
	4	Eff.	1.867	149	162
	5	Eff.	1.867	154	147
	6	Eff.	1.867	149	144
	7	Eff.	1.867	149	142
	8	Tracer	1.867	149	142
	9	Tracer	1.867	132	139

Table 17: Pressure drops of the second set of wheels

Exchanger	Test No.	Test type	Airflow rate (m^3/s)	Pressure drop (Pa)	
				Supply airstream	Exhaust airstream
W2: small	1	Eff.	0.371	142	214
	2	Eff.	0.371	139	207
	3	Eff.	0.259	100	144
	4	Tracer	0.371	169	197
	5	Tracer	0.371	154	164
W2: medium	1	Eff.	0.900	187	209
	2	Eff.	0.900	182	199
	3	Eff.	0.630	127	139
	4	Tracer	0.900	177	197
	5	Tracer	0.900	157	177
W2: large	1	Eff.	1.910	172	167
	2	Eff.	1.910	152	137
	3	Eff.	1.337	95	105
	4	Eff.	1.910	177	169
	5	Eff.	1.910	120	139
	6	Eff.	1.910	120	135
	7	Eff.	1.910	117	132
	8	Tracer	1.910	122	137
	9	Tracer	1.910	149	139

The accuracy of pressure measurement is 2.5 Pa. Because two pressure measurements are needed to obtain the pressure drop, the uncertainty of pressure drop is calculated to be 3.5 Pa, which is the same for all tests. This uncertainty meets the requirement of ASHRAE Standard, which specifies the following:

$$\frac{U(\Delta P_s)}{\Delta P_s} < 0.1 \qquad (29)$$

$$\frac{U(\Delta P_e)}{\Delta P_e} < 0.1 \qquad (30)$$

where, ΔP_s and ΔP_e are the pressure drop of the supply airstream and exhaust airstream, respectively.

Figures 35-38 show the results for the two sets of wheels, where the uncertainties are marked as error bars. For the purpose of enhanced readability, these figures show the results for the first three tests only.

For the first set of wheels (Figures 35 and 36), the pressure drop decreases from the small wheel to the large wheel. Because the error bars do not overlap, the pressure drop does not show consistency across different wheel sizes after accounting for test uncertainties. The comparison between Figure 35 and Figure 36 indicates that under the same test condition, the supply air pressure drop is essentially equal to the exhaust air pressure drop for a given wheel size, which is expected.

For the second set of wheels (Figures 37 and 38), the two airstreams show different trends. For the exhaust airstream, the pressure drop decreases from the small wheel to the large wheel (Figure 38). However, for the supply airstream, the pressure drop increases from the small wheel to the medium wheel and then decreases from the medium wheel to the large wheel. There is barely any overlap between error bars of different wheel sizes under the same test condition. The comparison between Figure 37 and Figure 38 show that for a given wheel size, the pressure drops of the two airstreams are quite different for many test conditions. For example, under the Test 1 condition, the small wheel has the pressure drop of 142 Pa in the supply air but 214 Pa in the exhaust airstream. It is not clear what caused the difference in pressure drop between the two airstreams.

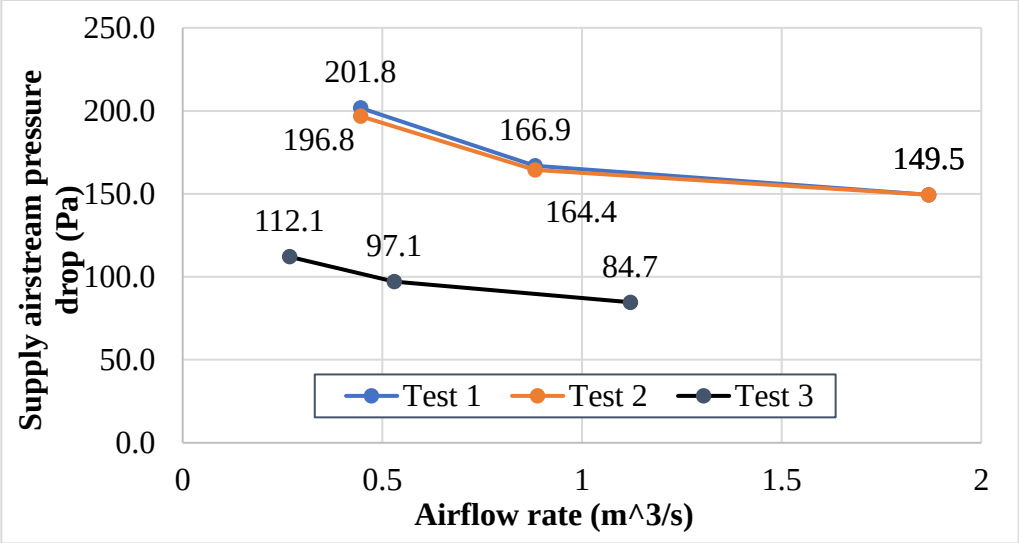

Figure 35: The change of supply air pressure drop with wheel size for the first set of wheels

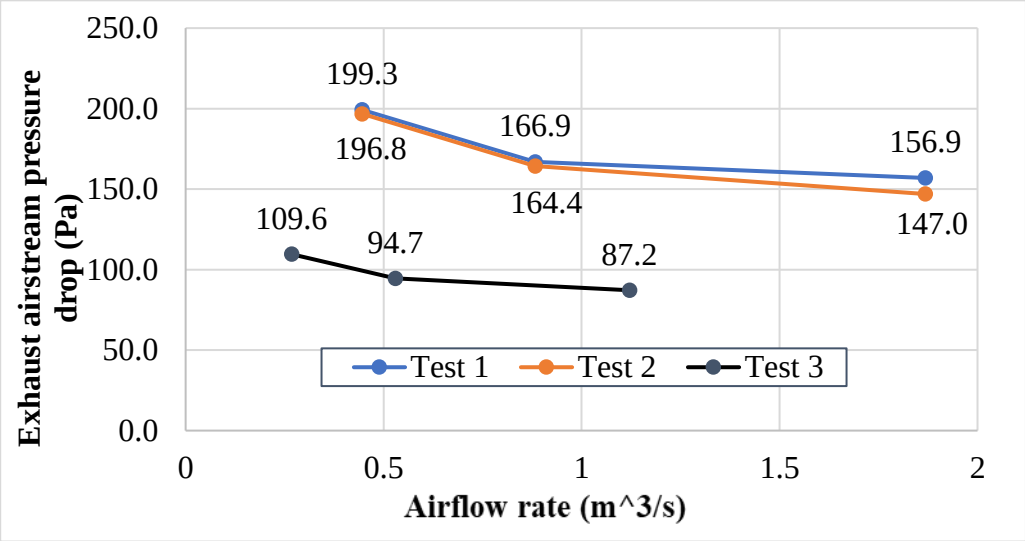

Figure 36: The change of exhaust air pressure drop with wheel size for the first set of wheels

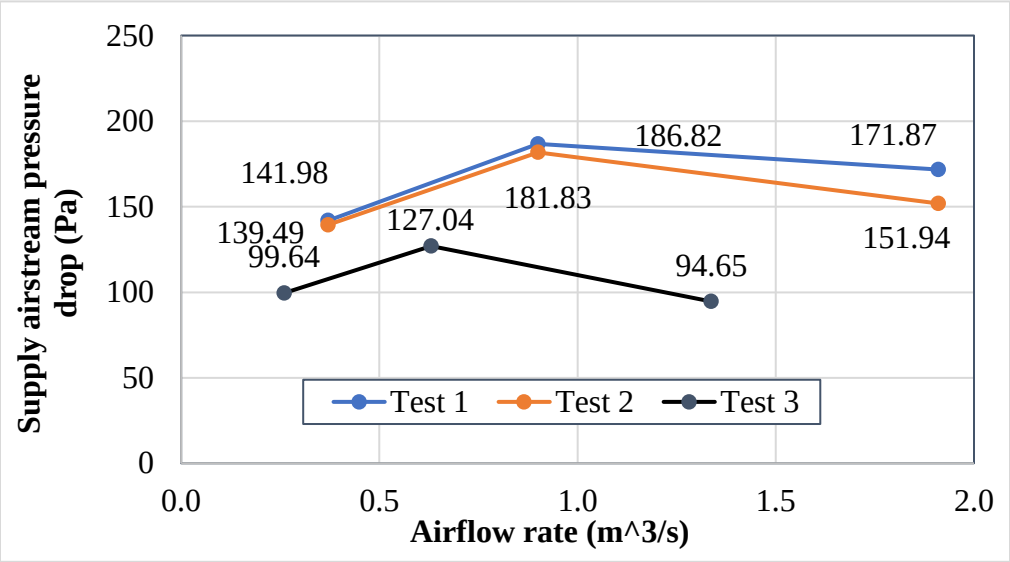

Figure 37: The change of supply air pressure drop with wheel size for the second set of wheels

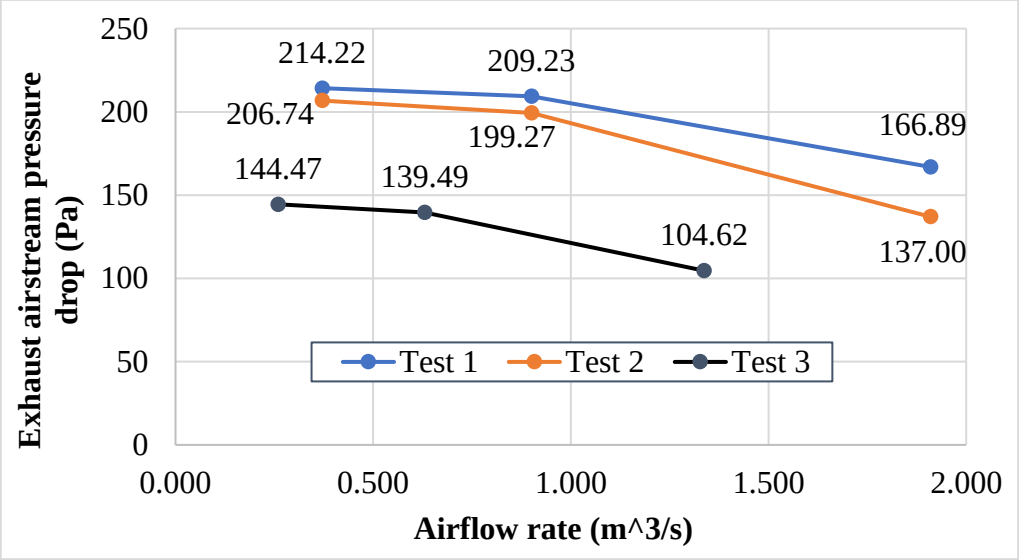

Figure 38: The change of exhaust air pressure drop with wheel size for the second set of wheels

Regarding the rating allowance for pressure drop, AHRI Standard 1060 states that test results for pressure drop shall not be greater than the published rating by 10%, or 12.5 Pa, whichever is greater. Therefore, based on the measured pressure drop, the corresponding range of pressure drop rating can be derived. Figures 39 and 40, and Figures 41 and 42 show the results for the two sets of wheels, where the rating ranges are marked as error bars. These figures indicate the following:

- For the first set of wheels, the rating ranges do not overlap between the small wheel and the large wheel.
- For the second set of wheels, there is no consistent observation of the overlap of rating ranges between different wheel sizes.
- Although the exception exists (i.e., the supply air pressure drop between the small wheel and the medium wheel), it is generally acceptable to provide the pressure drop rating for large wheels based on the test results of smaller wheels.

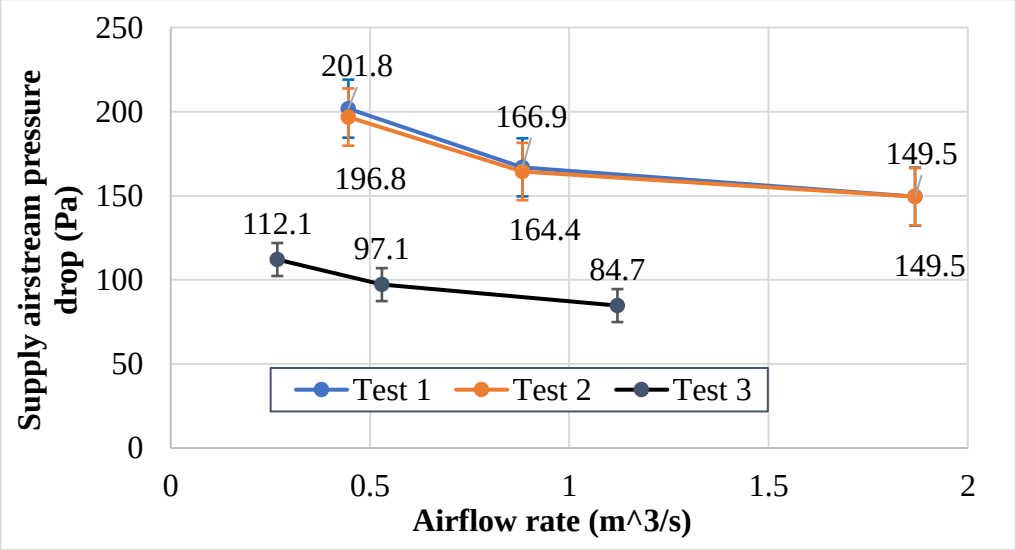

Figure 39: Acceptable rating ranges of supply air pressure drop for the first set of wheels

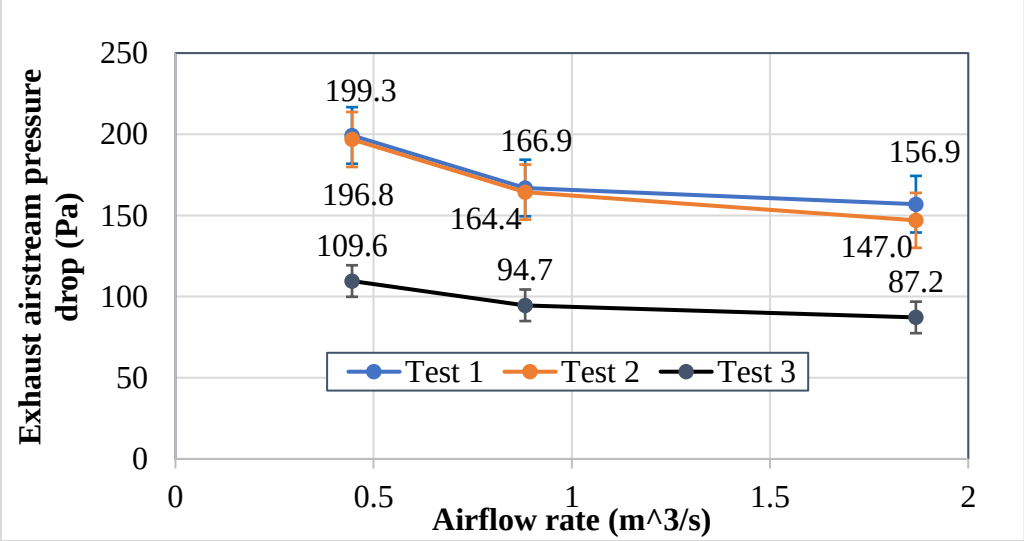

Figure 40: Acceptable rating ranges of exhaust air pressure drop for the first set of wheels

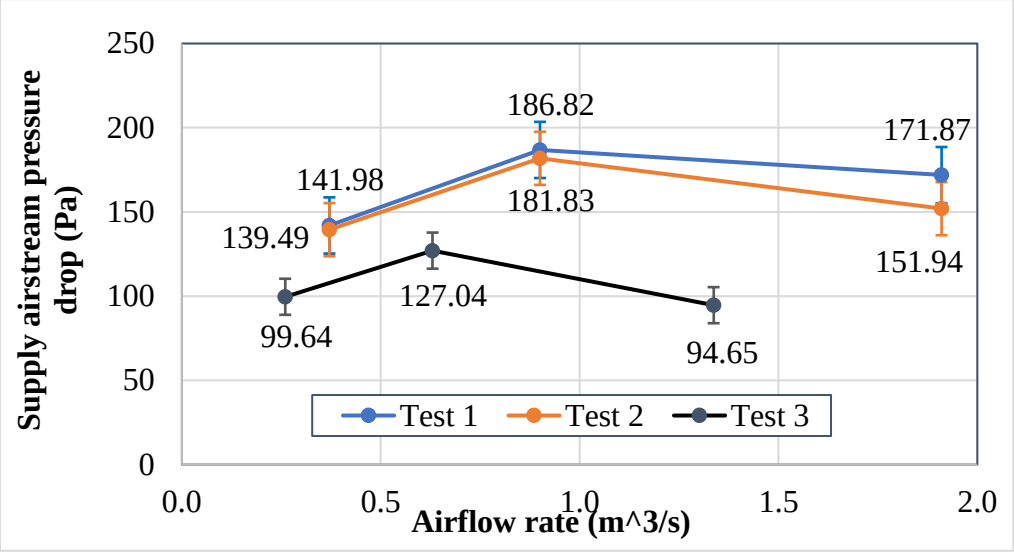

Figure 41: Acceptable rating ranges of supply air pressure drop for the second set of wheels

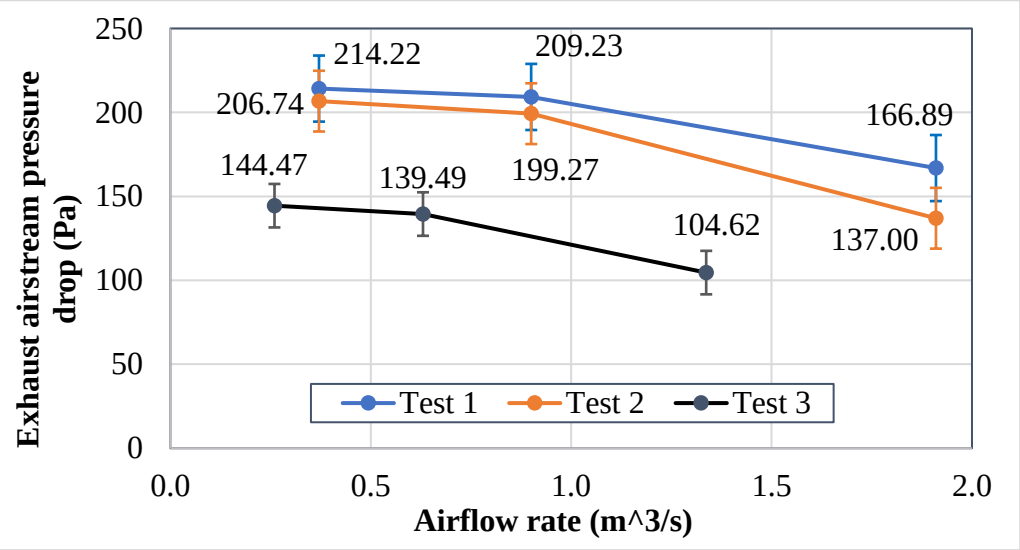

Figure 42: Acceptable rating ranges of exhaust air pressure drop for the second set of wheels

4.4 Validation of Selected Correlations from the Literature

The correlations proposed by Simonson and Besant (1999) needs a number of technical parameters about the product, such as the matrix mass, mass fraction of desiccant, volume fraction of desiccant, and surface area density of wheel. Unfortunately, the manufacturers regard those parameter values as proprietary information and cannot provide them for this work. Therefore, it is not feasible to validate the correlations from Simonson and Besant (1999) based

on our test results. However, certain elements of their work, such as H*, can still be used as mentioned previously.

The correlations proposed by Jeong and Mumma (2005) model the wheel effectiveness based on the air face velocity, the flow ratio between the two airstreams, the dry-bulb temperature and the relative humidity of entering air of the two airstreams, all of which are available from the test data. Therefore, the test results can be used to validate the correlations from Jeong and Mumma (2005). They developed two sets of correlations, one set for wheels with silicone gel and the other set for wheels with molecular sieve. Both sets of correlations were based on typical wheel characteristics such as rotational speed of 20 rpm and wheel depth of 200 mm. These characteristics are consistent with the second set of tested wheels only. Therefore, based on the test conditions for the second set of tested wheels, the correlations from Jeong and Mumma (2005) are applied. Figures 43 and 44 respectively compares the sensible effectiveness and latent effectiveness between the test results and the correlation results. These figures show the following:

- For the sensible effectiveness (Figure 43), the test results and the correlation results have quite large differences. The correlation results are approximately 10%~12% higher than the test results. On average, the difference is 11.87%.
- For the latent effectiveness (Figure 44), the test results and the correlation results match very well except for Test condition 4, which shows an almost 5% difference.

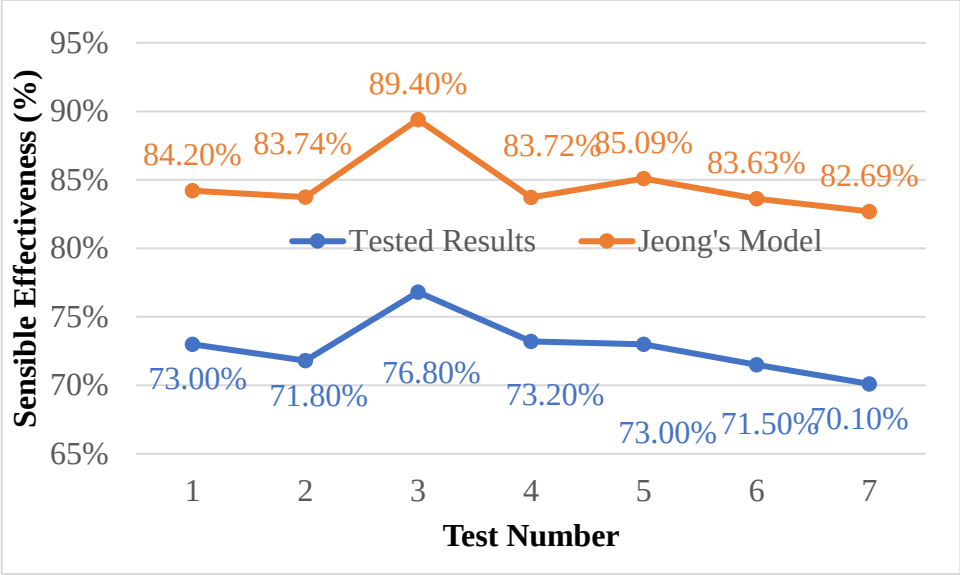

Figure 43: Comparison of the sensible effectiveness

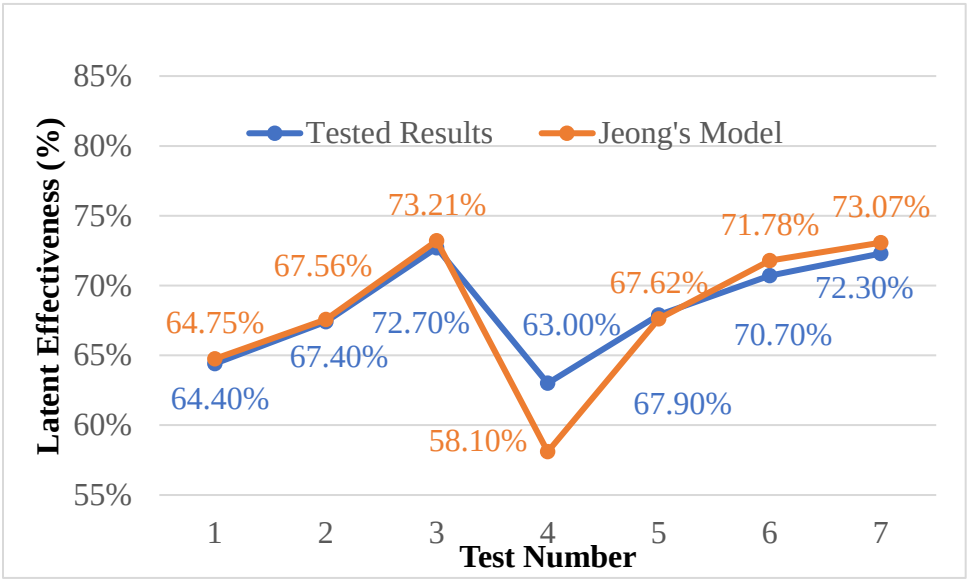

Figure 44: Comparison of the latent effectiveness

This is the first third-party effort to validate the correlations from Jeong and Mumma. Therefore, it is not possible to find sources from the literature that directly explain why there is a large difference between the test results and the correlation results. After some research, one possible reason may be the neglect of axial heat conduction when using the numerical heat and transfer model of energy wheels to develop the correlations. Figure 45 is from Simonson and

Besant (1999), where the dotted line shows the sensible effectiveness without considering the axial heat conduction and the straight line with triangular markers shows the sensible effectiveness with the consideration of axial heat conduction. These two lines are about 10% apart, which supports our explanation of the cause of the large difference between the test results and the correlation results. This demonstrates the importance of considering axial heat conduction when applying the numerical heat and mass transfer models for energy wheels.

Therefore, the original correlation equation for sensible effectiveness (Jeong and Mumma 2005) needs to be modified by decreasing 11.9%, the average difference between test results and the original correlation results. Equation 31 shows the modified correlation. Figure 46 compares the modified correlation results with the test results, which are very close with each other.

$$\varepsilon_s=(\alpha_0+\alpha_1(V_{si})+\alpha_2(T_{si})+\alpha_3(\emptyset_{si})+\alpha_4(Q_R)+\alpha_5(V_{si*}T_{si})+\alpha_6(V_{si*}\emptyset_{si})+\alpha_7(V_{si*}Q_R)+\alpha_8(T_{si*}\emptyset_{si})+\alpha_9(T_{si*}Q_R)+\alpha_{10}(\emptyset_{si*}Q_R)+\alpha_{11}(V_{si*}T_{si*}\emptyset_{si})+\alpha_{12}(V_{si*}T_{si*}Q_R)+\alpha_{13}(T_{si*}\emptyset_{si*}Q_R))\text{-}11.9\% \quad (31)$$

The modified correlation equation will be used in next chapter in a whole building simulation to understand to what extent that ignoring the impact of operating conditions on effectiveness could have on building energy simulation results. Because Jeong and Mumma (2005) performed cross-model validations in their work, the validation work presented in this section indirectly supports the models by Simon and Besant (1999b) and Freund et al. (2003).

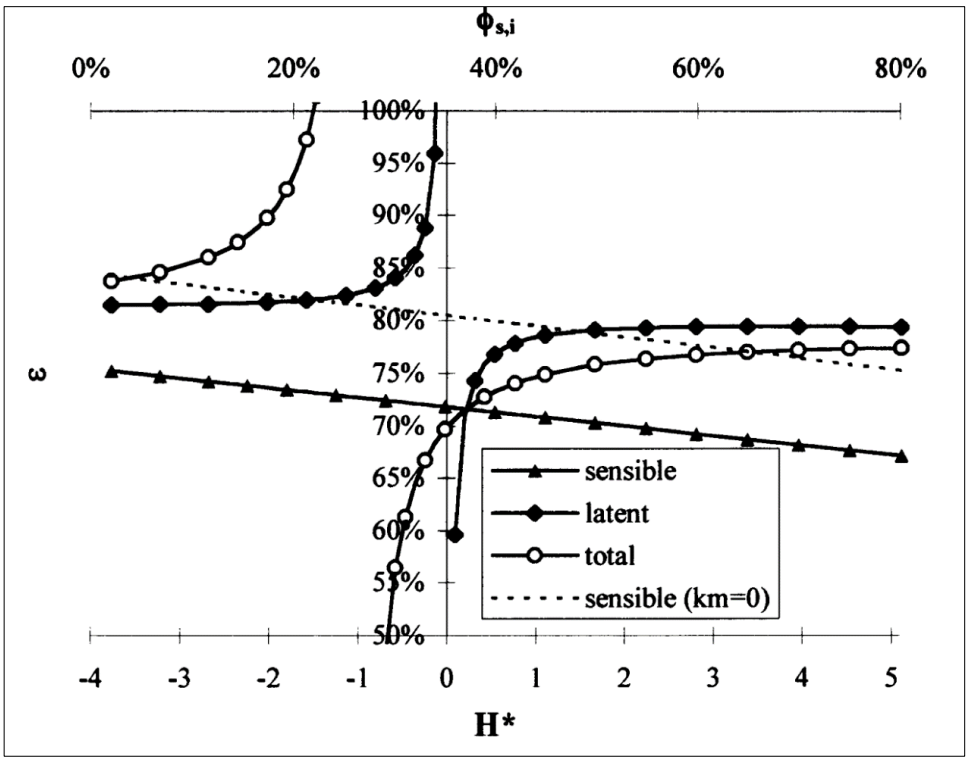

Figure 45: Effectiveness vs H* for hot test conditions (Simonson and Besant 1999)

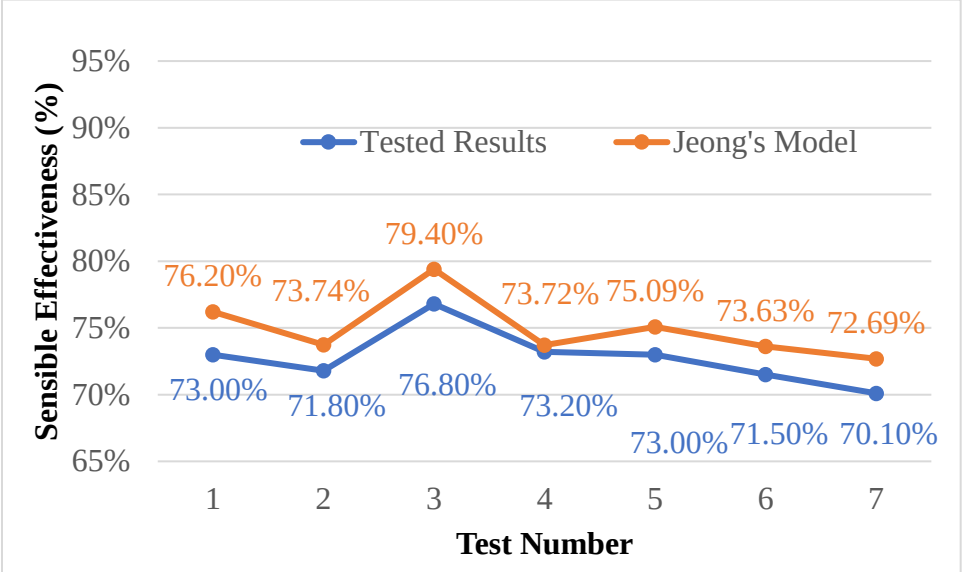

Figure 46: Comparison of the sensible effectiveness after considering axial heat conduction

Chapter 5: Impact of Effectiveness Extrapolation on Energy Simulation

Building simulation models are usually used to evaluate the benefits of applying air-to-air energy recovery in HVAC systems. The current practice is to simulate air-to-air energy recovery based on the rated performance while the impact of operating conditions on effectiveness is either simply ignored or not fully considered. No research has been performed to justify the current practice. In this chapter, the impact of effectiveness extrapolation on energy simulation is investigated using the whole building simulation program — EnergyPlus.

5.1 Building Model

A building model is needed to investigate the impact of effectiveness extrapolation on simulation results. Prototype building models have been developed by the Building Codes Program of the U.S. Department of Energy (DOE 2022). There are 16 prototype building models for different commercial building types such as office building, primary school, outpatient healthcare, and standalone retail. For each building type, a total of 19 EnergyPlus models exist for different climate zones, as defined in ASHRAE Standard 169 (ASHRAE 2021). The standalone retail building model is selected to be used in this work.

The standalone retail building has a rectangular footprint (54.2 m x 42.4 m), one floor, a total floor area of 2298 m^2 and a floor-to-ceiling height of 6.1 m. The building has windows on its front side, which accounts for 25% of the front façade area. Regarding the construction, the building has a slab-on-grade floor, concrete block walls and a built-up roof on metal deck. The thermal performance of building envelope meets the minimum requirement of ASHRAE Standard 90.1-2019 (ASHRAE 2019b). Figures 47 shows an axonometric projection of the building.

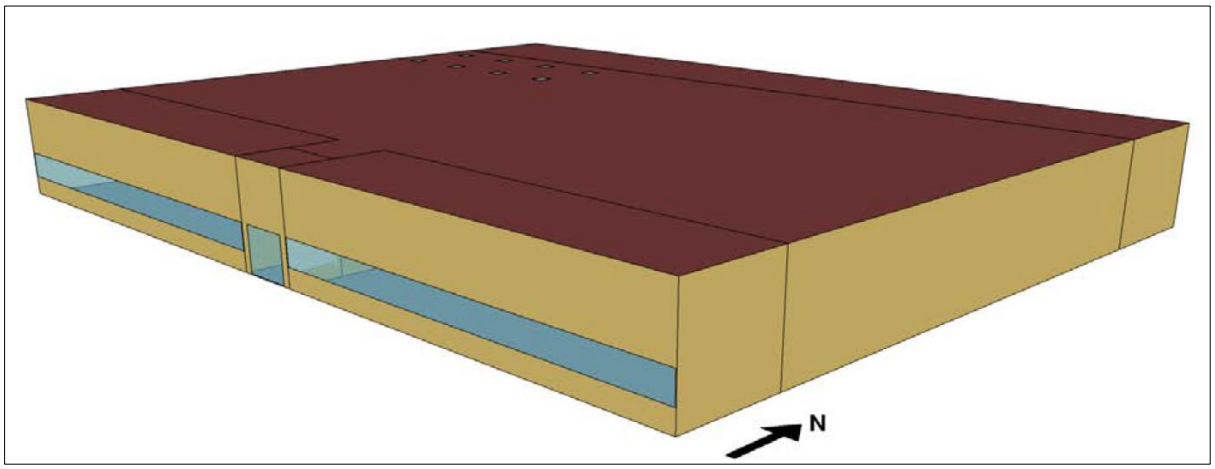

Figure 47: Standalone retail building shape (DOE 2022)

The building is divided into five thermal zones (Figure 48), including back space, core retail, point of sale, front retail and front entry. These five thermal zones respectively account for 16.5%, 70%, 6.5%, 6.5% and 0.5% of the total floor area. Internal loads (i.e., lighting, occupants, and plug loads) are modeled in these zones based on the relevant standards (e.g., ASHRAE Standard 90.1 and ASHRAE Standard 62.1) and typical practices.

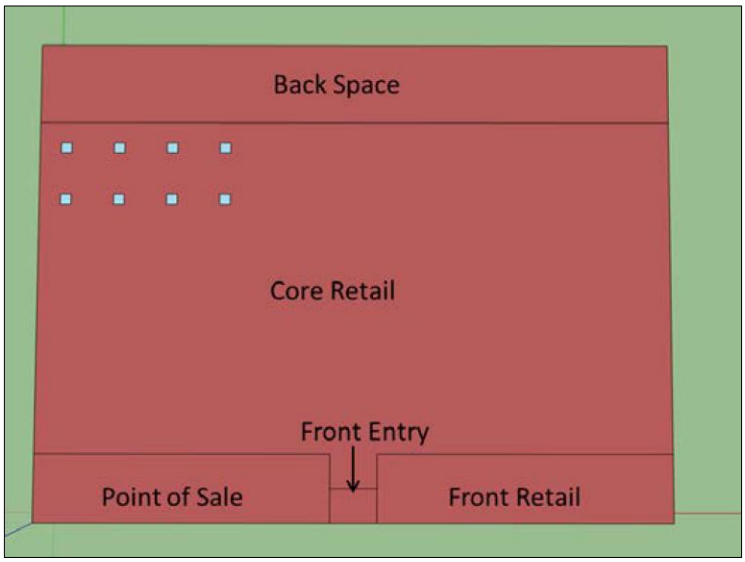

Figure 48: Thermal zoning (DOE 2022)

Except for the front entry that is served by a unit heater to address the heating loads, all other thermal zones are served by single-zone packaged rooftop air-conditioning units. Each roof unit is equipped with a two-stage cooling, a multi-speed supply fan, and a gas furnace.

The original prototype model for standalone retail buildings has been developed for different climates. Each climate is represented by one representative location in the simulation model. Only the warm and humid climate (i.e., climate zone 3A in ASHRAE Standard 169 and 90.1), with Atlanta, GA being its representative location, is selected in this work. Major reasons behind this selection include the following:

- The warm and humid climate is appropriate for the use of energy recovery. This climate also covers many areas in the U.S. (EIA 2012) and therefore, the findings from this work can be widely applicable.
- The use of air-to-air energy recovery in warm and humid climate usually does not require frost controls. As to be discussed later in Section 5.2, customized programs need to be developed to capture the impact of operating conditions on the effectiveness of energy exchangers. Because developing customized programs in EnergyPlus is error prone and time consuming, it is wise to minimize the scope of customization by avoiding frost controls, which must be considered in cold climates.

5.2 Modeling Air-to-Air Energy Recovery in EnergyPlus

EnergyPlus has two models for air-to-air energy recovery (both sensible and latent heat exchange) between two airstreams. These two models are HeatExchanger:AirToAir:SensibleAndLatent and HeatExchanger:Desiccant:BalancedFlow, which are called Objects in EnergyPlus models.

For the first model (Figure 49), the energy exchanger's thermal performance can be specified by providing the sensible and latent effectiveness at 75% and 100% of the rated supply airflow rate at two standard operating conditions. These two operating conditions refer to the winter heating condition and the summer cooling condition, which were used by AHRI before 2020 to rate the thermal performance of energy exchangers (see Table 5).

```
HeatExchanger:AirToAir:SensibleAndLatent,
  OA Heat Recovery 1,          !- Name
  FanAndCoilAvailSched,        !- Availability Schedule Name
  0.4333,                      !- Nominal Supply Air Flow Rate {m3/s}
  .76,                         !- Sensible Effectiveness at 100% Heating Air Flow {dimensionless}
  .68,                         !- Latent Effectiveness at 100% Heating Air Flow {dimensionless}
  .81,                         !- Sensible Effectiveness at 75% Heating Air Flow {dimensionless}
  .73,                         !- Latent Effectiveness at 75% Heating Air Flow {dimensionless}
  .76,                         !- Sensible Effectiveness at 100% Cooling Air Flow {dimensionless}
  .68,                         !- Latent Effectiveness at 100% Cooling Air Flow {dimensionless}
  .81,                         !- Sensible Effectiveness at 75% Cooling Air Flow {dimensionless}
  .73,                         !- Latent Effectiveness at 75% Cooling Air Flow {dimensionless}
  Outside Air Inlet Node Preheated,   !- Supply Air Inlet Node Name
  Heat Recovery Outlet Node,   !- Supply Air Outlet Node Name
  Relief Air Outlet Node,      !- Exhaust Air Inlet Node Name
  Heat Recovery Secondary Outlet Node,   !- Exhaust Air Outlet Node Name
  200.0,                       !- Nominal Electric Power {W}
  No,                          !- Supply Air Outlet Temperature Control
  Plate,                       !- Heat Exchanger Type
  None;                        !- Frost Control Type
```

Figure 49: HeatExchanger:AirToAir:SensibleAndLatent model (DOE 2021)

To obtain the operating effectiveness of the energy exchanger, the model calculates the average volumetric air flow rates through the exchanger at every simulation time step and then applies linear interpolation or extrapolation to determine the actual operating effectiveness of the energy exchanger based on the actual operating air flow ratio and the effectiveness values at 100% flow and 75% flow specified in the input. For example, the operating sensible effectiveness is calculated as (DOE 2021):

$$\varepsilon_{s,operatingFlow} = \varepsilon_{s,75\%Flow} + \left(\varepsilon_{s,100\%Flow} - \varepsilon_{s,75\%Flow}\right)\frac{FR-0.75}{1-0.75} \quad (32)$$

where, ε_s is the sensible effectiveness, FR is the ratio of the average operating volumetric airflow rate to the nominal airflow rate, the subscripts $operatingFlow$, $75\%Flow$, and

$100\%Flow$, respectively represents the operating flow condition, 75% of the nominal flow rate condition, and 100% of the nominal flow rate condition.

The above description indicates that the first model considers the impact of airflow rate on effectiveness, but it does not consider the impact of entering air properties (i.e., dry-bulb temperature and wet-bulb temperature) on effectiveness. Because it is not possible to change the effectiveness according to entering air properties, the first model cannot be used in this work.

The second model, HeatExchanger:Desiccant:BalancedFlow, considers the exchanger performance through a performance data object type called HeatExchanger:Desiccant:BalancedFlow:PerformanceDataType1 (Figure 50). This performance data object type calculates the regeneration air outlet temperature and humidity ratio based on the predefined correlation equations while the equation coefficients can be user-specified. For example, the equation for calculating the dry-bulb temperature of regeneration outlet air is defined as (DOE 2021):

$$RTO = b1 + b2 * RWI + b3 * RTI + b4 * \frac{RWI}{RTI} + b5 * PWI + b6 * PTI + b7 * \frac{PWI}{PTI} + b8 * V \quad (33)$$

Where,

RTO: regeneration outlet air dry-bulb temperature (°C)

RWI: regeneration inlet air humidity ratio (kg/kg)

RTI: regeneration inlet air dry-bulb temperature (°C)

PWI: process inlet air humidity ratio (kg/kg)

PTI: process inlet air dry-bulb temperature (°C)

V: air face velocity (m/s)

```
HeatExchanger:Desiccant:BalancedFlow,
  Desiccant Heat Exchanger 1,                !- Name
  OfficeHeatCoolAvail,                              !- Availability Schedule Name
  DXSystem 1 Mixed Air Node,                 !- Regeneration Air Inlet Node Name
  DX Cooling Coil Air Inlet Node,         !- Regeneration Air Outlet Node Name
  DX Cooling Coil Air Outlet Node,       !- Process Air Inlet Node Name
  DXSystem 1 Fan Air Inlet Node,          !- Process Air Outlet Node Name
  HeatExchanger:Desiccant:BalancedFlow:PerformanceDataType1, !- Heat Exchanger Performance Object
    Type
  HXDesPerf1;                                                !- Heat Exchanger Performance Name
```

Figure 50: HeatExchanger:Desiccant:BalancedFlow model (DOE 2021)

Another equation with the same format as Eq. 33 but with different coefficients is used to calculate the regeneration outlet air humidity ratio. Even though the second model captures the impact of inlet air properties on exchanger performance, it cannot be used in this work for the following reasons. First, the roles of the two air streams may switch during annual simulation. For example, the exhaust air is regarded as the regeneration air in summer but as the process air in winter. Second, Eq. 33 is totally different from Eq. 31, which is the performance correlation equation to be studied.

Because both of the two authentic models for air-to-air energy recovery in EnergyPlus cannot be used to support this research, a new strategy must be developed. Fortunately, EnergyPlus provides method for users to include customized models for HVAC components. The object Coil:UserDefined is used to model air-to-air energy recovery by using the two air connections: one connection for supply air and the other one for exhaust. Figure 51 shows how the object Coil:UserDefined for the air-to-air energy recovery in the packaged system serving the core retail.

```
Coil:UserDefined,

  PSZ-AC:2 OA Heat Recovery,  !- Name
  PSZ2 OA HR Model Program Manager,  !- Overall Model Simulation Program Calling Manager Name
  PSZ2 OA HR Init Program Manager,  !- Model Setup and Sizing Program Calling Manager Name
  2,                  !- Number of Air Connections
  PSZ-AC:2_OAInlet Node,  !- Air Connection 1 Inlet Node Name
  PSZ-AC:2 Heat Recovery Outlet Node,  !- Air Connection 1 Outlet Node Name
  PSZ-AC:2_OARelief Node,                  !- Air Connection 2 Inlet Node Name
  PSZ-AC:2 Heat Recovery Secondary Outlet Node,                  !- Air Connection 2 Outlet Node Name
  No;                 !- Plant Connection is Used
```

Figure 51: Coil:UserDefined for the air-to-air energy recovery in the packaged system serving the core retail

Customized programs using the Energy Management System (EMS) feature of EnergyPlus are then developed. Figure 52 shows the pseudocode of the implemented EMS program:

```
Get the entering air properties including dry-bulb temperature, humidity ratio, and mass flow rate
IF the air mass flow rate is 0
  Set the leaving air properties equal to the entering air properties
ELSE
  Calculate the sensible effectiveness based on Eq. 31. and latent effectiveness based on Eq. 21
  Calculate the leaving air properties
ENDIF
```

Figure 52: The pseudocode of the implemented EMS program

The customized programs have been implemented for all four packaged single-zone systems in the standalone retail model. To investigate the impact of effectiveness extrapolation on energy simulation, two simulation models are developed. One simulation model uses the performance correlation equation (Eq. 31 and Eq. 21) to assign the exchanger's effectiveness values at each simulation timestep. The second simulation model uses fixed effectiveness values which are calculated from Eq. 31 and Eq. 21 based on the standard operating conditions (Table 5). The results are presented next.

5.3 Energy Simulation Results

Table 18 summarizes the EnergyPlus simulation results for all four packaged single-zone system. The results include the natural gas energy consumption for heating, the electricity consumption for cooling and fan, and the relative difference between the two cases (with and without the consideration of operating conditions on exchanger effectiveness). This table shows the following:

- Ignoring the impact of operating conditions on exchanger effectiveness has negligible impact on cooling energy consumption. This indicates that the effectiveness values do not change much when the supply air needs to be cooled.
- Ignoring the impact of operating conditions on exchanger effectiveness has noticeable impact on heating energy consumption. Comparing with the case of using fixed effectiveness, the case of using effectiveness correlation has 3% less natural gas energy consumption for System 1, 18% less energy for System 2, and 5% less energy for Systems 3 and 4. The impact on System 2 is much higher than the other three systems. One possible reason is that the core retail may have a higher space air temperature (the same as the exhaust air inlet temperature for energy recovery) than the other three zones because the ratio of exterior envelop to floor area is much smaller for the core retail zone.

Table 18: EnergyPlus simulation results

System	Case	Energy consumption (MJ)		Difference	
		Natural gas	Electricity	Natural gas	Electricity
System 1 (back space)	Using effectiveness correlation	16614	41137	3%	0%
	Fixed effectiveness	17098	41127		
System 2 (core retail)	Using effectiveness correlation	8758	216290	18%	0%
	Fixed effectiveness	10709	215489		
System 3 (Point of sale)	Using effectiveness correlation	2562	30356	5%	0%
	Fixed effectiveness	2685	30376		
System 4 (front retail)	Using effectiveness correlation	4588	32177	5%	0%
	Fixed effectiveness	4805	32180		

Chapter 6: Conclusions

6.1 Summary

Buildings in the U.S. consumes about 40% of the total energy consumption, while HVAC equipment accounts for 40-60% of the energy consumption in buildings. So, using energy efficient HVAC equipment, air-to-air energy exchangers, can result in energy savings and capital cost reduction by downsizing the heating and cooling equipment. Air-to-air Energy exchangers come in different types and sizes, and they are categorized based on geometry, construction type, heat transfer, and the number of fluids. Some of the common types include rotary wheels, heat pipe, recuperators, and run-around loops. The operations manual of AHRI Standard 1060 allow large air-to-air energy exchangers with nominal air flow rates above 2.36 m^3/s to be rated the same as smaller exchangers, as long as both large and small exchangers have the same design and construction. However, the validity of AHRI's approach has not been investigated in the open literature. Also, most practitioners assume the certified performance of energy exchangers apply to a broad psychrometric range that are encountered in field operation. Many energy simulation software adopt the same assumption. However, laboratory studies are missing to evaluate the extent to which the heat exchanger performance varies with inlet air conditions

The work in this thesis includes reviewing the correlation methods used in the literature, compiling and analyzing test results data provided by Intertek, evaluating both the impact of energy exchanger sizes and operating conditions on performance based on laboratory testing results, comparing the laboratory test results with the correlations published in the literature, and using EnergyPlus software to estimate how much difference of simulated energy consumption can be caused by ignoring the impact of operating conditions on the performance of air-to-air energy exchangers. Major conclusions from this research include the following:

- The test results provide strong support of AHRI's extrapolation approach for effectiveness rating. Big wheels that cannot be accommodated by the laboratory testing facilities can have the same rated effectiveness as smaller wheels as long as they are in the same TSG.
- The test results support the current extrapolation approach in AHRI Standard 1060 for EATR rating when the pressure differential is zero. However, the approach could overestimate the EATR of large wheels with airflow rate more than 2.36 m^3/s if the pressure differential is -500 Pa or lower. This does not impose a problem from the consumer perspective because the overestimation of EATR conservatively evaluates the leakage performance of wheels. In addition, a positive value of pressure differential is more commonly used in the field to avoid leakage from the exhaust airstream to the supply airstream. With a positive pressure differential, the EATR is expected to be smaller than the EATR at zero pressure differential and the change of EATR with wheel size would be also smaller.
- The test results strongly support the AHRI extrapolation approach for OACF rating. Big wheels that cannot be accommodated by the laboratory testing facilities can have the same rated OACF as smaller wheels as long as they are in the same TSG.
- It is generally acceptable to provide the pressure drop rating for large wheels based on the test results of smaller wheels though the first set of wheels do not show strict consistency for all cases.
- Regarding the change of effectiveness with the operating conditions of supply and exhaust air, the sensible effectiveness decreases linearly as H* increases (the first set of wheels showed better linear relationship than the second set). The latent effectiveness and

the total effectiveness did not show strong and consistent relationship with H* for the two sets of wheels.

- Relative to entering air temperature, the air flow rate or the air face velocity has a higher impact on thermal performance. The effectiveness increased by 10% -13% for the first set of wheels after the reduction of air face velocity by 40%. The effectiveness increased by 6% -14% for the second set of wheels after the reduction of air face velocity by 30%.
- The test results have been used to validate the effectiveness correlations from Jeong and Mumma (2005). The latent effectiveness correlation matches well with the test results, but the sensible effectiveness correlation needs to be modified to match well with the test results.
- A customized model has been developed in EnergyPlus to investigate the impact of operating conditions on annual energy simulation. The simulation of a standalone retail building in Atlanta showed that ignoring the impact of operating conditions on exchanger effectiveness had a negligible impact on cooling energy consumption but deviated heating energy consumption by 5%-18%.

6.2 Future Work

This research could be extended in the future along the following aspects:

- The test results need to be communicated with both manufacturers who provided their wheels for testing. The manufacturer may provide insights on a couple of observations that cannot be easily explained. For example, it is unclear what caused the difference in pressure drop between the two airstreams for the second set of wheels.

- Because the test results showed different relationships between H* and the latent and total effectiveness values from the previous work (Simonson and Besant 1999), it is worthwhile to investigate the underlying reasons behind the above difference.
- In this work, the EnergyPlus simulation model was developed for only the warm and humid climate. Adding frost controls to the customized programs would enable the EnergyPlus model to be applicable in other climates.

References

Al-Hyari, L. and Kassai, M., 2021. Development of TRNSYS model for energy performance simulation of variable refrigerant flow air-conditioning system combined with energy recovery ventilation. International Journal of Green Energy, 18(4), pp.390-401.

AHRI, 2018. AHRI Standard 1060 (I-P): Performance Rating of Air-to-Air Exchangers for Energy Recovery Ventilation Equipment. Air-conditioning, Heating, & Refrigeration Institute, Arlington, VA.

AHRI, 2020. AHRI ERV OM: Air-to-Air Energy Recovery Ventilators Certification Program. Air-conditioning, Heating, & Refrigeration Institute, Arlington, VA.

ASHRAE, 2019a. ANSI/ASHRAE Standard 62.1-2019: Ventilation for Acceptable Indoor Air Quality. American Society of Heating, Refrigerating and Air-Conditioning Engineers, Atlanta, GA.

ASHRAE, 2019b. ANSI/ASHRAE Standard 90.1-2019: Energy Standard for Buildings Except Low-Rise Residential Buildings. American Society of Heating, Refrigerating and Air-Conditioning Engineers, Atlanta, GA.

ASHRAE, 2020a. ANSI/ASHRAE Standard 84-2020: Method of Testing Air-to-Air Heat/Energy Exchangers. American Society of Heating, Refrigerating and Air-Conditioning Engineers, Atlanta, GA.

ASHRAE, 2020b. Handbook of HVAC Systems and Equipment: Chapter 26: Air-to-Air Energy Recovery Equipment. American Society of Heating, Refrigerating and Air-Conditioning Engineers, Atlanta, GA.

ASHRAE, 2021. ANSI/ASHRAE Standard 169-2013: Climatic Data for Building Design Standards. American Society of Heating, Refrigerating and Air-Conditioning Engineers, Atlanta, GA.

ASME, 2013. ASME Standard PTC19.1-2005: Test Uncertainty. American Society of Mechanical Engineers, New York, NY.

Beccali, M., Butera, F., Guanella, R.A.R.S. and Adhikari, R.S., 2003. Simplified models for the performance evaluation of desiccant wheel dehumidification. International Journal of Energy Research, 27(1), pp.17-29.

BSI, 1997. Heat Exchangers – Test Procedures for Establishing the Performance of Air to Air and Flue Gases Heat Recovery Devices. BS EN 308, British Standards Institute.

Crawley, D.B., Hand, J.W., Kummert, M. and Griffith, B.T., 2008. Contrasting the capabilities of building energy performance simulation programs. Building and environment, 43(4), pp.661-673.

CSA, 2018. Standard Laboratory Methods of Test for Rating the Performance of Heat/Energy-Recovery Ventilators. CSA C439-18, Canadian Standards Association.

DOE, 2021. EnergyPlus Version 9.6 Documents: Engineering Reference. U.S. Department of Energy.

DOE, 2021. EnergyPlus Version 9.6 Documents: Input Output Reference. U.S. Department of Energy.

DOE, 2022. Prototype Building Models. Building Energy Codes Program. U.S. Department of Energy, available at https://www.energycodes.gov/prototype-building-models and accessed in April, 2022.

ECC, 2019a. Eurovent Certita Certification RS 8/C/001-2019: Rating Standard for the Certification of Air to Air Plate and Tube Heat Exchangers. Eurovent Certita Certification: Paris, France.

ECC, 2019b. Eurovent Certita Certification RS 8/C/002-2019: Rating Standard for the Certification of Air to Air Regenerative Heat Exchangers. Eurovent Certita Certification: Paris, France.

EIA, 2012. 2012 CBECS Survey Data. U.S. Energy Information Administration, available at https://www.eia.gov/consumption/commercial/data/2012/index.php?view=characteristics#b1-b2 and accessed in April, 2022.

EIA, 2021. November 2021 Monthly Energy Review. U.S. Energy Information Administration, available at https://www.eia.gov/totalenergy/data/monthly/pdf/mer.pdf and accessed in November, 2021.

Freund, S., Klein, S.A. and Reindl, D.T., 2003. A semi-empirical method to estimate enthalpy exchanger performance and a comparison of alternative frost control strategies. HVAC&R Research, 9(4), pp.493-508.

Fumo, N., Mago, P. and Luck, R., 2010. Methodology to estimate building energy consumption using EnergyPlus Benchmark Models. Energy and Buildings, 42(12), pp.2331-2337.

ICC, 2018. International Green Construction Code. The International Code Council.

IEA, 2019. The Critical Role of Buildings. International Energy Agency, available at https://www.iea.org/reports/the-critical-role-of-buildings and accessed in November, 2021.

ISO, 2014. "Heat Recovery Ventilators and Energy Recovery Ventilators — Method of Test for Performance". ISO 16494, International Organization for Standards.

Jeong, J.W. and Mumma, S.A., 2005. Practical thermal performance correlations for molecular sieve and silica gel loaded enthalpy wheels. Applied thermal engineering, 25(5-6), pp.719-740.

Jiru, T.E., 2014. Combining HVAC energy conservation measures to achieve energy savings over standard requirements. Energy and buildings, 73, pp.171-175.

Liu, J., Li, W., Liu, J. and Wang, B., 2010. Efficiency of energy recovery ventilator with various weathers and its energy saving performance in a residential apartment. Energy and Buildings, 42(1), pp.43-49.

Nugent, Ciara, and Data Visualization by Emily Barone. Why Net Zero Targets May Not Stop Climate Change. Time, Time, https://time.com/6113845/net-zero-climate-pledge-impact/.

Rasouli, M., Simonson, C.J. and Besant, R.W., 2010. Applicability and optimum control strategy of energy recovery ventilators in different climatic conditions. Energy and Buildings, 42(9), pp.1376-1385.

Simonson, C.J. and Besant, R.W., 1999. Energy wheel effectiveness: part I—development of dimensionless groups. International Journal of Heat and Mass Transfer, 42(12), pp.2161-2170.

Simonson, C.J. and Besant, R.W., 1999. Energy wheel effectiveness: part II—correlations. International Journal of Heat and Mass Transfer, 42(12), pp.2171-2185.

Simonson, C.J., 1998. Heat and moisture transfer in energy wheels (Doctoral dissertation, University of Saskatchewan).

Stiesch, G., Klein, S.A. and Mitchell, J.W., 1995. Performance of rotary heat and mass exchangers. HVAC&R Research, 1(4), pp.308-323.

Thornton, B.A., Wang, W., Lane, M.D., Rosenberg, M.I. and Liu, B., 2009. Technical support document: 50% energy savings design technology packages for medium office buildings (No. PNNL-19004). Pacific Northwest National Lab. (PNNL), Richland, WA (United States).

Zeng, C., Liu, S. and Shukla, A., 2017. A review on the air-to-air heat and mass exchanger technologies for building applications. Renewable and Sustainable Energy Reviews, 75, pp.753-774.

Zhou, Y.P., Wu, J.Y. and Wang, R.Z., 2007. Performance of energy recovery ventilator with various weathers and temperature set-points. Energy and Buildings, 39(12), pp.1202-1210.